

CPEE 2025

Computational Problems of Electrical Engineering 2025

Rašovice, Czech Republic, September 10th - 12th, 2025.

PROCEEDINGS

LIST OF PAPERS

A Comparative Study of Gaussian and Hyperbolic Secant Repulsive Fields in APF-Based Path Planning

Ihor Berizka, Ivan Karbovnyk

Adaptive 3D Augmentation in StyleGAN2-ADA for High-Fidelity Lung Nodule Synthesis from Limited CT Volumes

Oleksandr Fedoruk, Konrad Klimaszewski, Michal Kruk

Adjustable underground system tile generation for application in computer games

Izabella Antoniuk

Analysis of a Chaotic Oscillator Signal Using the Quaternion Short-Time Fourier Transform

Lukasz Makowski

Application and comparison of various neural networks for the detection and measurement of pest feeding symptoms in plants

Michal Kruk

Augmented Reality in Industrial applications

Petr Kropík, Jan Matoušek, Jakub Racek, Lenka Šroubová

Biological parameters controlled by Background Static Magnetic Field

Marek Bajtoš, Roman Radil, Ladislav Janoušek, Nhat Dang, Jason Keller, Hakki Gurhan, Frank Barnes, Isabel Lopez de Mingo

Compressing a Siamese Vision Transformer for Efficient Full-Reference Image Quality Assessment

Bartosz Kwaśny

Convolutional Kolmogorov Arnold Networks as an accurate alternative to Convolutional Neural Networks for rule discovery

Patryk Ferenc, Sebastian Górka, Maciej Michalski, Bartosz Chaber

Design and Development of a Multi-Modal Bioamplifier

Branko Babusiak, Maros Smondrk, Lubomir Trpis, Ladislav Janousek

Determination of operational parameters of an asynchronous electric drive with sequential reactive power compensation

Vasyl Malyar, Orest Hamola, Volodymyr Maday, Ivanna Vasylchyshyn

Dynamic Response of Energy System under Contingency: A Simulation-Based Assessment

Zagdkhorol Bayasgalan, Nomin Lkhgvasuren, Munkh-Erdene Oyundelger, Tsetsgee Bayasgalan

Electrical Engineering in Wartime: Perspectives on Ukraine's Energy Sector

Oksana Hoholyuk, Ivanna Vasylychshyn, Iryna Moroz, Myroslav Sabat

Enhancing Insulator Inspection: A YOLO and DETR Approach to Image-Based Defect Detection

Dominika Pacek, Zuzanna Krawczyk-Borysiak

Epileptic Seizure Detection from EEG Signal: A Subject-Dependent Approach

Kamil Grzegorzewski, Andrzej Majkowski, Marcin Kołodziej

Evaluating the Effect of Tattoos on Photoplethysmography Imaging Perfusion Monitoring

Michal Labuda, Patrik Durajka, Veronika Wohlmuthova, Jan Seleng

Evaluation of selected missing data imputation methods for two photovoltaic grid generation datasets

Robert Szmurło, Krzysztof Siwek

Evaluation of Specific Absorption Rate in Ear Tissue After Exposure to Electromagnetic Fields from Cell Phone

Zuzana Psenakova

Experimental Study of Extremely Low Frequency and Static Magnetic Fields in Household Devices Using a Cost-Effective Portable Magnetometer

Veronika Wohlmuthova, Michal Labuda, Lubomir Trpis, Mariana Benova

Explainability of Convolutional Neural Network: overview of methods

Magdalena Markowicz, Piotr Podgórski, Jan Kruszyński, Karim Sonbul, Krzysztof Siwek

Fast Adaptation to New Classes of Odors in the Electronic Nose

Krzysztof Siwek, Tomasz Grzywacz, Piotr Witkowski, Tran Hoai Linh

Foreign Exchange Rate Forecasting Using Machine Learning Approaches: A Signal-Based Perspective

Artur Krupa, Konrad Maleńczak

Four types of short circuit currents in three-phase electrical networks

Jacek Korytkowski, Kazimierz Mikołajuk, Krzysztof Siwek, Andrzej Toboła

Higher harmonics presence in experiments with LF MF exposure of biological samples

Roman Radil

Hybrid ensemble of cnn-based classifiers in melanoma recognition

Stanisław Osowski, Fabian Gil

Hybrid Order-Aware CNN–Vision–Language Model for LN-RADS–Based Lymph-Node Diagnosis

Grzegorz Gwardys, Maciej Jurewicz, Jarosław Kurek, Cezary Chudobiński, Bartosz Świdorski

Impedance-frequency characteristics of surface dry EEG electrodes using an agar-based phantom

Lubomir Trpis, Maros Smondrk, Veronika Wohlmuthova, Branko Babusiak

Influence of external electromagnetic field at mains frequency 50Hz on pacemakers

Michal Gala, Milan Smetana, Ivana Galova, Mariana Benova

Interactive Visualization of Data from a Ceramic Printer

Lenka Šroubová, Karel Slobodník, Petr Kropík, Jakub Racek, Michal Prokeš, Jan Rejzek

Limits of Large Language Models in Map Navigation and Spatial Reasoning

Bartosz Sawicki, Tomasz Leś

Low-Cost Randomness Extraction from Power Line Voltage Signal

Piotr Witkowski, Bartosz Sawicki

Machine learning In Industrial Cyberthreat Detection

Mateusz Praniuk, Maksymilian Roj, Janusz Pochmara, Krzysztof Kolanowski, Aleksandra Świetlicka

Mathematical Model of a Saturated Synchronous Motor in Orthogonal d-q Axes as an Element of a Microgrid

Oksana Hoholyuk, Petro Gogolyuk

Measurement of variation characteristics on electric field peak value due to microgap ESD

Ken Kawamata, Shinobu Ishigami, Osamu Fujiwara

Methodology for assesment of induced voltage on human body in the vicinity of overhead electric lines

Roman Radil

Modeling of the Electric Field Generated in the Human Body by Endovascular Electrodes

Jacek Starzyński

Modelling of Chaotic Phenomena in an Electric Arc Furnace System

Piotr Witkowski, Radosław Roszczyk

Multi-agent Peer Review Committee for Automated Policy Analysis and Ethical Rules Enforcement

Estera Kot, Santhosh Kumar Ravindran, Krzysztof Siwek, Zuzanna Krawczyk-Borysiak, Weronika Nitecka

Multi-task learning and its optimization methods

Karol Wojciechowski, Grzegorz Gwardys, Maciej Jurewicz, Bartosz Świdorski

On generation of adversarial sequences for recurrent neural networks in classification and forecasting

Rafał Zan, Bartosz Chaber

Secondary Electron Emission modeling for 2nd Townsend Coefficient estimation in Julia/CUDA

Wiktor Łodyga, Bartosz Chaber, Jacek Starzyński

Simplified Information Coding System for Use in Emergency Situations

Dmitro Trushakov

Study of Digital Twin Technology for SCADA System Simulation and Analysis

Nomin Lkhgvasuren, Zagdkhorol Bayasgalan, Wolfram Hardt, Uranchimeg Tudevdagva

Subject-Independent Classification of SSVEP Signals for Brain-Computer Interface Applications

Przemysław Wiszniewski, Marcin Kołodziej, Andrzej Majkowski

Survey on Racing simulators as an environment for reinforcement learning

Jacek Wójtowicz, Krzysztof Siwek

Three-State Monitoring Circuit for Sensor Operation in Automation Systems

Agnieszka Choroszucho, Norbert Waśkiewicz

Wavelet Transform denoising in application for EM field signal acquisition

Adam Jósko, Jacek Starzyński

A Comparative Study of Gaussian and Hyperbolic Secant Repulsive Fields in APF-Based Path Planning

Ihor Berizka, Ivan Karbovnyk

*Ivan Franko Lviv National University, 107 Tarnavskoho Str, Lviv, 79013, Ukraine,
ihor.berizka@lnu.edu.ua*

Abstract—This study compares two probabilistic variants of APFM—Gaussian-based and Hyperbolic Secant-based—by modeling their repulsive forces differently and evaluating their performance in simulated static environments using TurtleBot3 and Gazebo. Metrics such as path length and execution time were collected across repeated trials and analyzed using statistical tools, including kernel density estimation and non-parametric significance testing.

Where A_k is scaling parameter, θ_k corresponds to the central angle of the k_{th} obstacle, σ_k is half of angle occupied by the k_{th} obstacle.

Both algorithms were tested in static environments with repeated runs, measuring computational time and path length. Statistical analysis included kernel density estimation and non-parametric tests.

I. INTRODUCTION

Autonomous mobile robots rely on efficient obstacle avoidance algorithms to navigate dynamic environments safely. While the Artificial Potential Field Method (APFM) [1] is widely used for local path planning, traditional implementations suffer from local minima and computational inefficiencies. This study compares two probabilistic APFM modifications—Gaussian and Hyperbolic Secant-based—to address these limitations and improve real-time performance.

The main idea of method is in calculation of 3 fields: attractive (drives robot towards target locations), repulsive (generated by obstacles to repel robot away) and total field. Safe direction is determined by finding argument of the minimum of the total field. Recent modifications involve simplifying mathematical models and moving toward scalar functions instead of vectors [2]. Authors conducted studies with Gaussian function to calculate potential. In previous works we conducted research using Laplace function [3]. In this exercise we do comparative study of potentials based on Gauss function and on Hyperbolic secant function [4].

II. METHODS

A simulation framework was developed using ROS2/Gazebo with the TurtleBot3 platform. The Gaussian APFM (ODG-PF) and Hyperbolic Secant APFM were mathematically modeled, with key differences in repulsive force calculations. The Gaussian variation calculates repulsive force according to equation (1), while Hyperbolic Secant utilizes equation (2).

$$f_k(\theta_i) = A_k * \exp\left(-\frac{(\theta_k - \theta_i)^2}{2\sigma_k^2}\right) \quad (1)$$

$$f_k(\theta_i) = A_k * \operatorname{sech}\left(\frac{\pi}{2} * \frac{\theta_k - \theta_i}{\sigma_k}\right) \quad (2)$$

III. RESULTS

The Hyperbolic Secant APFM demonstrated superior responsiveness, with sharper repulsive forces near obstacles and rapid decay at greater distances. This resulted in smoother trajectories (validated over 28 navigation steps) and fewer abrupt corrections compared to Gaussian APFM. Computational benchmarks revealed a negligible 2–3% overhead for the hyperbolic secant function, which was mitigated by compiler optimizations.

IV. DISCUSSION & CONCLUSION

The hyperbolic secant's heavy-tailed distribution enhances local obstacle avoidance without distorting global paths, making it ideal for dynamic environments. Its computational efficiency aligns with real-time requirements, though further optimization is needed for resource-constrained systems. Future work will explore hybrid implementations and dynamic obstacle scenarios.

REFERENCES

- [1] B. Sciliano, O. Khatib, *Springer Handbook of Robotics*, 2nd ed. Springer-Verlag Berlin Heidelberg, (2016), pp. 1189-1190.
- [2] Jang-Ho Cho, Dong-Sung Pae, Myo-Taeg Lim, Tae-Koo Kang. "A Real-Time Obstacle Avoidance Method for Autonomous Vehicles Using an Obstacle-Dependent Gaussian Potential Field" in *Journal of Advanced Transportation*, 2018. [Online]. Available: <https://doi.org/10.1155/2018/5041401>.
- [3] Berizka I, Karbovnyk I, "Computational Evaluation of Laplace Artificial Potential Field Methods for Real-Time Obstacle Avoidance in Gazebo", ISSN: 2524-0382 (print), 2707-0069 (online). 2025. *Advances in Cyber-Physical Systems (ACPS)*. Volume 10, Number 1. P. 1-9, <https://doi.org/10.23939/acps2025.01.001>.
- [4] I. Berizka, I. Karbovnyk, "Simulation-Based Evaluation of Hyperbolic Secant Potential Field for Real-Time Obstacle Avoidance", to be published in *Ukrainian Journal of Information Technology*, accepted for publication, June 2025.

Adaptive 3D Augmentation in StyleGAN2-ADA for High-Fidelity Lung Nodule Synthesis from Limited CT Volumes

1st Oleksandr Fedoruk

*Institute of Information Technology
Warsaw University of Life Sciences
Warsaw, Poland*

*Department of Complex Systems
National Centre for Nuclear Research
Otwock, Poland
0000-0002-9433-2430*

2nd Konrad Klimaszewski

*Department of Complex Systems
National Centre for Nuclear Research
Otwock, Poland*

0000-0003-0741-5922

3rd Michał Kruk

*Institute of Information Technology
Warsaw University of Life Sciences
Warsaw, Poland*

0009-0005-0460-6039

Abstract—Generative adversarial networks (GANs) require substantial amounts of data for successful training. Training GANs on volumetric medical data, such as computed tomography (CT) or positron emission tomography (PET), presents additional challenges due to limited data availability.

A slice-wise generation approach can mitigate this limitation by treating each slice as an individual training object; however, it requires additional methods to preserve the anatomical features of the generated samples.

Adaptive discriminator augmentation (ADA) provides another means to improve generation quality with limited data. ADA dynamically adjusts the augmentation strategy during training to optimize data diversity and model performance based on feedback from the learning process.

Specialized architectures, such as three-dimensional (3D) StyleGAN for vascular magnetic resonance angiography (MRA), cyclic PET-CT GAN, and U-Net-based 3D GANs, demonstrate the potential of tailored discriminators and priors. However, these architectures remain largely unexplored under adaptive 3D augmentations. Prior applications of ADA in two-dimensional (2D) StyleGAN2 suggest stabilization benefits that this work extends to full 3D images.

We present a 3D StyleGAN2-ADA implementation with the full set of original augmentation techniques adapted for volumetric data. The network architecture is derived from the original 2D version, with all operations redefined for volumetric processing.

Experiments are conducted on the NoduleMNIST3D dataset, which contains chest CT scans of lung nodules divided into two classes. A total of 590 voxel-based samples are used for training. Due to the extremely small dataset size, we investigate the effect of volumetric ADA on training quality and stability. Two augmentation pipelines are compared: one with color-based augmentations only, and another incorporating all available augmentations (including color, geometric transformations, image-space filtering, and corruptions). Results are further compared with the original 2D StyleGAN2-ADA architecture trained slice-wise, with slices concatenated into 3D images.

We evaluate generation quality using the Kernel Inception Distance (KID) and the Learned Perceptual Image Patch Sim-

ilarity (LPIPS), and perform class-wise comparisons based on the applied augmentation pipeline. Results indicate that an aggressive augmentation strategy improves training stability, reduces the risk of mode collapse, and enables realistic synthetic object generation from very small training datasets, while better preserving anatomical features compared with slice-wise training using the 2D architecture.

Index Terms—Generative adversarial networks (GAN), 3D deep learning, Adaptive discriminator augmentation (ADA), volumetric medical imaging, computed tomography (CT), medical image synthesis, lung nodules

We gratefully acknowledge Polish high-performance computing infrastructure PLGrid (HPC Center: ACK Cyfronet AGH) for providing computer facilities and support within computational grant no. PLG/2024/017410

Adjustable underground system tile generation for application in computer games

1st Izabella Atoniuk

*Department of Artificial Intelligence, Institute of Information Technology
Warsaw University of Life Sciences – SGGW*

Warsaw, Poland

izabella_antoniuk@sggw.edu.pl

Index Terms—Blender Geometry Nodes, Cellular Automata, Underground System Generation, User-Guided Procedural Generation, Procedural Generation for Games.

I. PROCEDURAL UNDERGROUND SYSTEM GENERATION

In this paper a comprehensive pipeline for interactive edition of underground systems, for application in computer games is explored. The method focuses on creating a usable dungeon layout, with separate, interactive tiles, allowing dynamic edition, without the need to regenerate the entire system. In the field of procedural content generation for games, the topic of fast and effective methods for procedural scene modelling grows increasingly important. Ability to check different ideas on the fly, and evaluate various alternatives for the word fragments is especially essential during the design stages, when different options need to be evaluated. If such elements are created manually, preparing even simple system can take hours. At the same time, using methods with too little human input, might results in content, that do not meet the basic requirements. Solution presented in this paper aims to address this problem: creating an interactive algorithm, allowing fast, user-guided generation.

The used methodology focuses on interactivity, using simple commands, incorporated in the Blender environment. Presented algorithm creates individual, equally sized tiles, in which system shape is represented. User can then expand the system, by adding new tiles, directly next to the original one. Prepared methodology facilitates both automatic update of connections between different system components, as well as manual edition of them. Each tile can be regenerated at will, and data representation allows for the creation of multilevel systems with complex structures. The content of the tile can be either fully generated, or be based on user defined sketch, outlining the main system components. If used, the images are assigned to individual tiles, and the resulting system can have both user defined, and automatically generated components. This is necessary for applications such as computer games, as often the designers might have general outline of some parts of the system, while they still need to work through different ideas for other areas.

For the tile generation part, user has few different options. Approach based on Cellular Automata is used to generate interesting, cave-like shapes, using similar methodology as the

one presented in [1]. Different method, using dynamic shape expansion, with possibility to enforce symmetry, similar as in [2], [3] is used for generating room shapes that resemble human-designed dungeons. There is also a possibility to combine both shapes. The entire solution is prepared using Blender application, with Geometry Nodes tool, custom scripts and in-app menu allowing system edition in real time. The prepared algorithm is capable of expanding the system, generating tiles according to user specification, and introducing on the fly modifications to its structure and shape. Since everything is prepared in the 3D modelling application, each modification is immediately visible. Additionally, the resulting system is built from actual 3D models, that can be easily transferred to other applications (i.e. various game engines), as well as further edited within the Blender application.

Resulting systems can contain complex space representation. Proposed methodology can be used both during the design process to evaluate different ideas quickly, as well as to generate basic system shape for further edition. The terrain can also be used for simple game, or to test game mechanics. Due to the interactive generation, any changes can be introduced quickly, and the designer can easily modify any parts of the system, that do not meet the game requirements. Presented solution is also capable of storing the final result as a set of points, in order to use it as a base for in-engine generation (i.e. if the user would want to build the resulting system from custom components). Overall the presented methodology provides a fast and interactive approach to user-guided procedural scene generation, producing visually interesting results, represented in 3D environment, with possibility for further edition as well as incorporation of created system (or parts of it) into further game development pipeline.

REFERENCES

- [1] I. Atoniuk, "Procedural generation of cave-like tiles with cellular automata and blender geometry nodes," in *2024 25th International Conference on Computational Problems of Electrical Engineering (CPEE)*. IEEE, 2024, pp. 1–4.
- [2] I. Antoniuk and P. Rokita, "Procedural generation of multilevel dungeons for application in computer games using schematic maps and l-system," in *Intelligent Methods and Big Data in Industrial Applications*. Springer, 2018, pp. 261–275.
- [3] I. Antoniuk, P. Hoser, and D. Strzemiwilk, "L-system application to procedural generation of room shapes for 3d dungeon creation in computer games," in *Advances in Soft and Hard Computing*. Springer, 2019, pp. 375–386.

Analysis of a Chaotic Oscillator Signal Using the Quaternion Short-Time Fourier Transform

Lukasz Makowski

Faculty of Electrical Engineering
Warsaw University of Technology
Warsaw, Poland

<https://orcid.org/0000-0002-4586-6890>

Abstract—A real-valued signal from a chaotic oscillator is embedded into quaternions using orthogonal components and analyzed via QSTFT with left-multiplied exponential kernels.

Index Terms—Signal analysis, Nonlinear dynamical systems, Quaternions

I. INTRODUCTION

Signals from chaotic generators exhibit strong nonlinearities and rich, often unpredictable dynamics. Their analysis, even when using methods such as phase space reconstruction, entropy measures, or Lyapunov exponents, typically relies on real- or complex-valued representations, which may not fully capture the multidimensional nature of chaotic behavior.

II. QUATERNIONS

Quaternions extend complex numbers into a four-dimensional number system comprising one real and three linearly independent imaginary units, denoted by \mathbf{i} , \mathbf{j} , and \mathbf{k} .

A general quaternion is expressed as:

$$q = a + b\mathbf{i} + c\mathbf{j} + d\mathbf{k} \quad (1)$$

where $a, b, c, d \in \mathbb{R}$.

The imaginary units satisfy the multiplication rules:

$$\mathbf{ijk} = \mathbf{i}^2 = \mathbf{j}^2 = \mathbf{k}^2 = -1 \quad (2)$$

and are pairwise non-commutative, e.g., $\mathbf{ij} = \mathbf{k}$, whereas $\mathbf{ji} = -\mathbf{k}$.

In quaternion signal processing, the imaginary components are used to embed higher-dimensional signal features, such as the gradient $\nabla(\cdot)$, the Hilbert transform $\mathcal{H}(\cdot)$, or multi-channel inputs.

III. METHODOLOGY

Chaotic oscillator used in this research was designed by Keuninckx et. al. as described in [1] and then considered as a possible signal source for Physically Unclonnable Function (PUF) for Internet of Things devices [2]. The robustness of a PUF derived from a chaotic oscillator critically depends on understanding its fine-grained temporal behavior, for which quaternionic signal analysis offers a structured, multidimensional approach.

The real-valued input signal from the chaotic oscillator serves as the foundation for computing quaternion components, which are mapped onto the imaginary components of the quaternion space, corresponding to the \mathbf{i} , \mathbf{j} , and \mathbf{k} axes.

Figure 1 visualizes a representative time slot of the resulting quaternion components after subsequent normalization, Gram-Schmidt orthogonalization, and windowing using a Tukey window with a taper parameter $r = 0.2$.

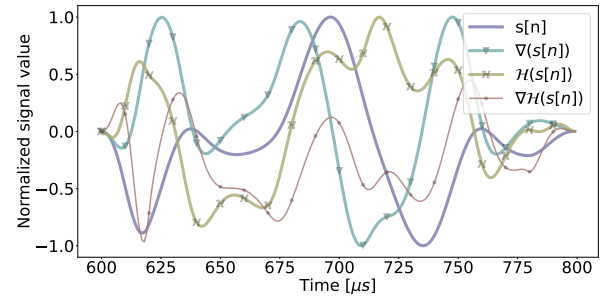


Fig. 1. Example of a quaternion signal segment after preprocessing (embedding, normalization, orthogonalization, windowing), forming the input to QSTFT.

Let $s[n] \in \mathbb{H}$ be a quaternion-valued discrete-time signal indexed by $n \in \mathbb{Z}$, and let $w[m] \in \mathbb{R}$ be a real-valued window function of length M . The Quaternion Short-Time Fourier Transform (QSTFT) of $s[n]$ is defined as:

$$\mathcal{Q}[r, n] = \sum_{m=0}^{M-1} w[m] s[n+m] e^{-\mu \omega_r m} \quad (3)$$

where $r = 0, 1, \dots, M-1$ is the frequency bin index, and $\omega_r = \frac{2\pi r}{M}$ is the corresponding angular frequency. The exponential kernel $e^{-\mu \omega_r m}$ rotates the signal about the selected, fixed quaternion axis μ , thus forming a hypercomplex generalization of the STFT.

REFERENCES

- [1] L. Keuninckx, G. Van der Sande, J. Danckaert, "Simple Two-Transistor Single-Supply Resistor-Capacitor Chaotic Oscillator", *IEEE Transactions on Circuits and Systems II: Express Briefs*, vol. 62, no. 9, pp. 891-895, Sept. 2015, doi: 10.1109/TCSII.2015.2435211
- [2] L. Makowski, "Evaluation of computational performance of PUF implementation for IoT device authentication", *Przegląd Elektrotechniczny*, 101 (2025), No. 3, pp. 229-232, doi: 10.15199/48.2025.03.53

Application and comparison of various neural networks for the detection and measurement of pest feeding symptoms in plants

Oleksandr Fedoruk
Institute of Information Technology
Warsaw University of Life Sciences
Warsaw, Poland
0000-0002-9433-2430

Anna Wlazło
Institute of Biology
Warsaw University of Life Sciences
Warsaw, Poland
0000-0001-5417-4119

Ewelina Złotkowska
Institute of Biology
National Centre for Nuclear Research
Otwock, Poland
0000-0001-7751-3072

Marcin Filipecki
Institute of Biology
Warsaw University of Life Sciences
Warsaw, Poland
0000-0003-4107-2484

Konrad Klimaszewski
Department of Complex Systems
National Centre for Nuclear Research
Otwock, Poland
0000-0003-0741-5922

Michał Kruk
Institute of Information Technology
Warsaw University of Life Sciences
Warsaw, Poland
0009-0005-0460-60

Climate change and the withdrawal of many biocidal substances from agricultural use are increasing the pressure to improve crop plant varieties to enhance their resistance to pests, diseases, and weather conditions. A major bottleneck in developing new varieties is the expert, objective, quantitative, and high-throughput assessment of plant susceptibility to specific pests. The advances in digital photography enable the use of AI models at various resolutions of pest-infected plant images. In this report, we present the capabilities of the models in detecting specific eggs of the two-spotted spider mite (*Tetranychus urticae*) on thale cress leaves (*Arabidopsis thaliana*) and damages caused by the same pest on maize leaves (*Zea mays*). Both the number and surface area of feces, as well as the extent of damage, are parameters proportional to the plant's susceptibility to the pest. However, their irregular shapes, varying surface areas, and coloration similar to various leaf impurities complicate precise detection and pose challenges for neural network models. The imaging of leaves differing in size and shape was performed using a specially configured Leica Thunder Imager System consisting of a stereo microscope with a camera and fully motorized XY-Scanning Stage. Image acquisition was performed using reflected light under $25\times$ magnification. A full leaf scan included approximately five hundred images of neighboring and partially overlapping pictures, which were merged automatically after scanning with the imaging system software. The images of abaxially and adaxially scanned leaf surfaces were exported to TIFF. To detect and measure symptoms of pest feeding damage on plants using machine learning, especially deep learning, different architectures were considered. These models differ in their goals (detection, segmentation, classification, regression) and complexity. In our work, a few models were tested: YOLO (Fast and accurate, well-suited for edge devices), Faster R-CNN (More accurate but slower) and Mask R-CNN. The results are presented in terms of accuracy, sensitivity, specificity, as well as recognition speed, since the work serves as a preliminary step toward developing an application that will enable farmers to identify threats.

Augmented Reality in Industrial applications

Petr Kropík

*Department of Electrical and Computational Engineering
University of West Bohemia in Pilsen
Pilsen, Czech Republic
pkropik@fel.zcu.cz*

Jakub Racek

*Department of Electrical and Computational Engineering
University of West Bohemia in Pilsen
Pilsen, Czech Republic
racekj@fel.zcu.cz*

Jan Matoušek

*Department of Electrical and Computational Engineering
University of West Bohemia in Pilsen
Pilsen, Czech Republic
jan2002@students.zcu.cz*

Lenka Šroubová

*Department of Electrical and Computational Engineering
University of West Bohemia in Pilsen
Pilsen, Czech Republic
lsroubov@fel.zcu.cz*

Abstract—This paper presents the design and implementation of interactive visualization techniques for dynamic spatial data in augmented and mixed reality (AR/XR) on the Microsoft HoloLens 2 headset. The system visualizes robot work zones, sensor data, and various environmental information that can be measured or generated in real time. Key areas of development include efficient data transfer between devices and the AR headset, integration of gesture controls, and the creation of ergonomic user interfaces specifically designed for industrial applications.

Index Terms—augmented reality, AR/XR, interactive visualization, spatial data, HoloLens 2, robotic systems, ergonomics, real-time interaction

I. INTRODUCTION

Interactive visualization is essential for electrical engineering devices. Augmented reality (AR) enhances design and prototyping with realistic visualizations for early flaw detection and deepens the understanding of physical fields for optimization and safety. In education, AR provides intuitive hands-on training, while for diagnostics and maintenance, it offers real-time visual guidance to improve efficiency. It also allows for impactful marketing and safe, risk-free training in hazardous scenarios. [1]

This paper examines the development and application of AR-based visualization tools for both industry and educational institutions.

II. INTERACTIVE VISUALIZATION APPLICATION

The application developed at the Department of Electrical and Computational Engineering allows users to interactively visualize 3D digital models of electrical engineering devices in augmented reality, complete with descriptive information, animations, and behavioral data. It supports both measured and dynamically computed data to aid decision-making. Users can interact with virtual prototypes in real-world settings, visualizing work zones [2], sensor ranges, physical fields like temperature, and receive assembly/disassembly instructions. The system also enables safety training through the simulation

of hazardous environments, making it applicable for both industrial and educational purposes.

Ongoing development focuses on efficient data transmission and processing, integrating intuitive voice and gesture controls, automatic real-world objects recognition, and developing predictive methods using digital twins. This comprehensive solution leverages augmented reality for visualizing, interacting with, and analyzing spatial data in industrial and educational contexts.



Fig. 1. AR model and real device

III. CONCLUSION

This paper demonstrates an effective AR application for visualizing dynamic spatial data. The system enhances understanding and efficiency in industrial and educational settings through intuitive, real-time interaction.

ACKNOWLEDGMENT

This research has been supported by the internal project of the University of West Bohemia in Pilsen and the SGS-2024-025 University Student Project.

REFERENCES

- [1] Morales Méndez, G.; del Cerro Velázquez, F. Impact of Augmented Reality on Assistance and Training in Industry 4.0: Qualitative Evaluation and Meta-Analysis. *Appl. Sci.* 2024, 14, 4564. <https://doi.org/10.3390/app14114564>
- [2] Matoušek Jan, Modular manipulator with feedback control (written in Czech), final bachelor's degree project, Faculty of Electrical Engineering, University of West Bohemia in Pilsen, 2025.

Biological parameters controlled by Background Static Magnetic Field

Marek Bajtos, Roman Radil, Ladislav Janoušek
Department of Electromagnetic and Biomedical Engineering
Faculty of Electrical Engineering and Information Technology, University of Zilina
Zilina, Slovak Republic
marek.bajtos@feit.uniza.sk,
ladislav.janousek@feit.uniza.sk,
radil@feit.uniza.sk

Nhat Dang, Jason Keller, Hakki Gurhan, Frank Barnes
Department of Electrical, Computer and Energy Engineering, University of Colorado Boulder,
Boulder, Colorado, USA
nhat.dang@colorado.edu,
hakki.gurhan@colorado.edu,
jason.keller@colorado.edu,
barnes@colorado.edu

Isabel Lopez de Mingo
Centro de Tecnología Biomédica (CTB), Universidad Politécnica de Madrid (UPM), 28223 Madrid, Spain
Escuela Técnica Superior de Ingenieros de Telecomunicación (ETSIT), Universidad Politécnica de Madrid (UPM), 28040 Madrid, Spain
isabel.lopez@ctb.upm.es

Abstract — This study presents experimental findings demonstrating that changes in Static Magnetic Field (SMF) in presence of 16.5 Hz time varying magnetic field with amplitude of 9.81 μT can alter the growth rates of HT-1080 fibrosarcoma cells in vitro, accompanied by a theoretical explanation of possible underlying mechanisms. Results indicate that these changes in SMF can both increase and decrease the growth rates, in addition to altering membrane potential and calcium ion (Ca^{2+}) concentrations (Fig. 1). These effects are hypothesized to arise from changes in chemical reaction rates mediated by changes in Zeeman shifting. The growth rates of fibrosarcoma cells were significantly modulated during 4-day exposures to SMFs with a different amplitude.

An exposure system is placed in each chamber to independently control the electromagnetic fields. The Mu-metal shielding ensures minimal interference from external magnetic sources, creating a controlled and uniform magnetic environment. This design aligns with the MagShield apparatus described by Vučković et al. (2024), which integrates Helmholtz coils within mu-metal enclosures to enhance field uniformity and reproducibility. The system supports simultaneous experimental and control conditions using separate chambers, a critical feature for minimizing confounding variables in biological assays. Such isolation is essential, as variations in geomagnetic fields can significantly impact experimental outcomes [Portelli et al., 2013]. The exposure system consists of a 4-faced acrylic box with sides measuring 16.5 cm, featuring an exterior Helmholtz coil. The selection of the most suitable Helmholtz coil geometry depends on the specific application, with trade-offs between magnetic field homogeneity and power consumption [Restrepo et al., 2017]. The top and bottom windings are 6 cm apart, with each winding layer occupying 1.75 cm. Remington PN155 wires (polyurethane-coated, 155 °C) at 22 AWG connect to an external signal generator through openings in the Mu-metal box located at the top surface corners.

Further data reveal concurrent changes in membrane potential and Ca^{2+} concentrations, emphasizing the role of cellular bioenergetics in magnetic field-induced growth modulation. Differences between normal and diseased tissues offers potential therapeutic applications. HT-1080

fibrosarcoma were chosen for high recurrence rates and well-established culturing procedures.

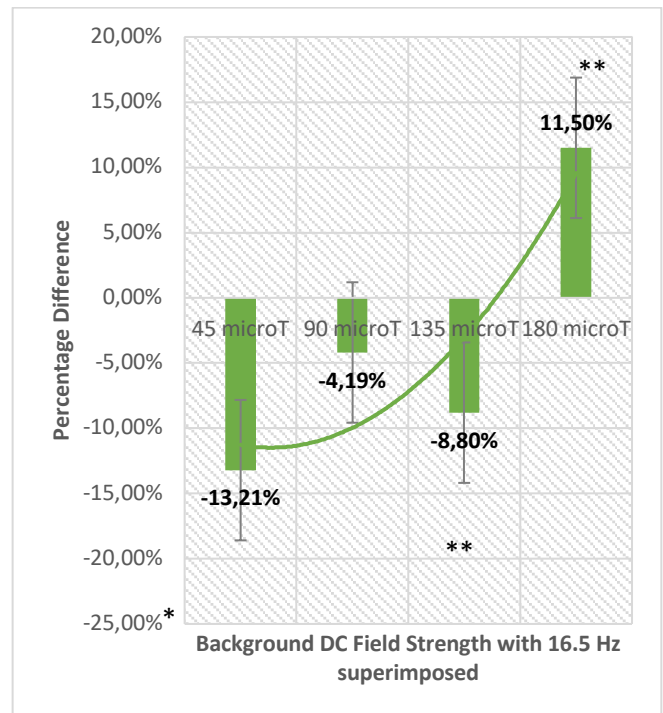


Fig. 1. The percentage difference between the growth rate of the treated and control as a function of the Background Static magnetic field of the treated sample with a 16.5 Hz, 9.81 μT superimposed AC field

- [1] Vučković, J., Gurhan, H., Gutierrez, B., Guerra, J., Kinsey, L. J., Nava, I., et al. (2024). Construction and application of a static magnetic field exposure apparatus for biological research in aqueous model systems and cell culture. *Bio Protoc.* 14, e5077.
- [2] Portelli, L. A., Schomay, T. E., & Barnes, F. S. (2013). Inhomogeneous background magnetic field in biological incubators is a potential confounder for experimental variability and reproducibility. *Bioelectromagnetics*, 34, 337–348.
- [3] Restrepo, A. F., Franco, E., Cadavid, H., & Pinedo, C. R. (2017). A comparative study of the magnetic field homogeneity for circular, square, and equilateral triangular Helmholtz coils. In *2017 International Conference on Electrical, Electronics, Communication, Computer, and Optimization Techniques (ICEECCOT)* (pp. 13–20). IEEE.

Compressing a Siamese Vision Transformer for Efficient Full-Reference Image Quality Assessment

Bartosz Kwaśny^{1,2} and Izabella Antoniuk¹

¹Department of Artificial Intelligence, Institute of Information Technology

Warsaw University of Life Sciences – SGGW

Warsaw, Poland

kwasnybartosz@proton.me

Abstract—Image Quality Assessment (IQA) aims to automate the process of determining image quality in a manner consistent with human perception. Specifically, Full-Reference IQA works by comparing an image to its reference, presumed to be free of distortions affecting the perceived quality. There are many approaches to FR-IQA, including subjective methods like MOS, traditional methods such as PSNR or SSIM, and also deep-learning based, often employing Convolutional Neural Networks (CNNs) or Vision Transformers (ViTs). Deep-learning based methods have been shown to model perceived quality better than traditional methods while being less time-consuming than subjective ones. However, such methods often rely on many different neural network layers and techniques in order to achieve the best possible predictions, resulting in resource-heavy solutions. There is a need for deep-learning based approaches that achieve strong performance while being efficient in terms of model size, inference time and energy usage. Such efficient solutions can be deployed in real-time scenarios, such as quality assessment of image transmission or compression methods. Moreover, such approach allows a more efficient deep-learning models training, like image super-resolution, restoration and many more. Finally, it is possible to deploy on-device solutions where energy efficiency is necessary.

Vision Transformers (ViTs) [1] have been shown to achieve strong performance in computer vision tasks, being adopted as alternatives to Convolutional Neural Networks (CNNs). However, their high parameter count in comparison to CNNs makes ViTs more challenging to implement in systems that are resource-constrained or require real-time data processing. This work investigates model compression methods to allow Siamese ViT designed for FR-IQA to be more efficient in terms of model size, inference time and energy usage, while trying to maintain model performance. To address the challenges, it is necessary to explore core compression strategies: model quantization [2], pruning [3] and knowledge distillation [4]. Quantization reduces the numerical precision of weights and activations (e.g. from 32-bit floating point to 8-bit integer) providing memory usage and inference latency reduction. Pruning works by removing redundant neural network weights or entire layers in order to simplify calculations. Knowledge distillation is used to transfer knowledge from a larger "teacher" neural network to a smaller, more efficient "student" model while retaining task-specific accuracy.

The primary objective is to develop a compressed Siamese ViT for FR-IQA starting from an already trained baseline employing a Siamese ViT with a Fully Connected ranking head. Model performance will be measured using correlation with human ratings included in FR-IQA datasets using Pearson and correlation coefficients. Additionally, model size, parameters count, inference latency and energy usage will be tested.

Index Terms—Image analysis, Image quality, Artificial Neural Networks, Vision transformers, Neural network compression

REFERENCES

- [1] A. Dosovitskiy, L. Beyer, A. Kolesnikov, D. Weissenborn, X. Zhai, T. Unterthiner, M. Dehghani, M. Minderer, G. Heigold, S. Gelly, J. Uszkoreit, and N. Houlsby, "An image is worth 16x16 words: Transformers for image recognition at scale," 2021. [Online]. Available: <https://arxiv.org/abs/2010.11929>
- [2] D. Du, G. Gong, and X. Chu, "Model quantization and hardware acceleration for vision transformers: A comprehensive survey," 2024. [Online]. Available: <https://arxiv.org/abs/2405.00314>
- [3] M. Zhu, Y. Tang, and K. Han, "Vision transformer pruning," 2021. [Online]. Available: <https://arxiv.org/abs/2104.08500>
- [4] G. Hinton, O. Vinyals, and J. Dean, "Distilling the knowledge in a neural network," 2015. [Online]. Available: <https://arxiv.org/abs/1503.02531>

Convolutional Kolmogorov Arnold Networks as an accurate alternative to Convolutional Neural Networks for rule discovery

Patryk Ferenc

Warsaw University of Technology
Warsaw, Poland

Sebastian Górka

Warsaw University of Technology
Warsaw, Poland

Maciej Michalski

Warsaw University of Technology
Warsaw, Poland

Bartosz Chaber

Warsaw University of Technology
Warsaw, Poland
bartosz.chaber@pw.edu.pl

Abstract—The paper attempts to train a Convolutional Kolmogorov-Arnold Network on a grid of cells changing their state according to the Game of Life cellular automaton rules. We compare which Convolutional Kolmogorov-Arnold Network (ConvKAN) architectures can be trained to reproduce the rules based only on the presented subsequent grids of cells. The Kolmogorov-Arnold Networks are compared with their classical Convolutional Neural Network (CNN), which lacks trainable activation functions. The ultimate goal is to use ConvKAN to also recover the Finite Difference Time-Domain stencil of wave equation.

In total, we have trained 12 ConvKAN and CNN architectures with different layers and different activation functions. Each architecture has been trained many times to estimate a mean network accuracy to reduce the influence of the random initialization of the network’s parameters. A simple, two-layer ConvKAN with 54 total trainable parameters has achieved almost 100% accuracy on test data, whereas a larger, two-layer CNNs (45 and 89 trainable parameters) performed slightly worse.

The ultimate goal of the research was to assess the ability to visualize ConvKAN trained activation functions to gain insight into the recovered rules of the cellular automaton. Indeed, the ConvKAN model reflects the rules in its parameters, considering each cell’s neighborhood while taking the central cell’s state with a different weight.

The results of the paper might as well be extended to other types of deterministic systems, and we believe they could attempt to discover rules in such systems. This method could help model real-world devices and processes that might be substituted with neural networks but with the additional advantage of having a trainable activation function.

Index Terms—Kolmogorov Arnold Networks, Convolutional Neural Networks, Neural Network Interpretability

Model accuracy To ensure robust comparisons, all models were trained 10 times with different random seeds to mitigate the effects of weight initialization. The results in Table I report:

- Mean accuracy, taken as the best-performing run per model;
- Epochs to convergence, averaged across successful runs;
- Number of converged runs, indicating how often the model reached 100% accuracy.

TABLE I: RESULTS OF TRAINING CNNs AND CONVKANs TO PREDICT THE NEXT STEP IN THE CONWAY’S GAME OF LIFE. SQUARE KERNEL SIZE OF 3.

Model	Layers	Filt.	Mean Acc.	Epochs to 100%	Models @100%	Params
Rand ^(a)	—	—	50%	—	—	—
CNN-A	2 ^(b)	1	73%	—	0	12
CNN-B		2	81.3%	8	3	23
CNN-C		4	94.7%	8.57	7	45
CNN-D		8	96.4%	8.71	7	89
CNN-E	2 ^(c)	1	81.7%	7	3	13
CNN-F	3 ^(d)	2	84.5%	5	2	31
CKAN-A	1 ^(e)	1	74.9%	—	0	45
CKAN-B	1 ^(f)	1	74.9%	—	0	46
CKAN-C	3 ^(g)	2	100%	2.4	10	140
CKAN-D		4	100%	1.8	10	342
CKAN-E		8	100%	1.5	10	938
CKAN-F	2 ^(h)	1	99.6%	3.38	8	54

^(a)Random classifier following a discrete uniform distribution. ^(b)A 3×3 convolution layer with ReLU activation, followed by a 1×1 convolution layer with sigmoid activation as output.

^(c)Same as ^b, but with PReLU activation in the first layer. ^(d)A convolution layer followed by two 1×1 convolutions. All layers use PReLU, except the output layer, which uses sigmoid.

^(e)A single ConvKAN layer with sigmoid activation. ^(f)A single ConvKAN layer with PReLU activation.

^(g)A ConvKAN layer followed by two 1×1 convolutions. All layers use PReLU, except the output layer, which uses sigmoid. ^(h)A ConvKAN layer with PReLU activation, followed by a 1×1 ConvKAN layer with sigmoid activation.

The results in Table I show that a minimal CNN with a single filter (13 parameters) and PReLU activation achieves a mean accuracy of 81.7% but does not always converge. For ReLU-based CNNs, at least two filters are required for any successful convergence. Models with more filters generally show higher convergence rates and faster training.

KAN-based models tend to have more parameters than their CNN counterparts. However, larger ConvKAN models (three layers, ≥ 2 filters) consistently reach 100% accuracy in all runs, converging in as few as 1.5–2.4 epochs.

Design and Development of a Multi-Modal Bioamplifier

Branko Babusiak, Maros Smondrk, Lubomir Trpis, Ladislav Janousek

Abstract— This paper presents the design of a versatile, low-cost bioamplifier for acquiring biopotentials. The system was tested with electrocardiogram signals, demonstrating its ability to capture high-quality data. Its compact design and low cost make it suitable for both research and clinical applications, particularly in settings with limited budgets.

I. INTRODUCTION

This paper presents the design and implementation of a versatile, low-cost bioamplifier for acquiring biopotentials from cardiac, neural, and muscular activities. The system integrates an ADS1298 analog front-end with an ATmega328PB microcontroller to enable efficient data acquisition and processing. Key features include: support for multiple sensing modalities: wet, dry, and capacitive electrodes; real-time electrode contact impedance measurement; configurable acquisition parameters via client application, and real-time signal visualization and data logging.

II. METHODS

The bioamplifier's analog front-end provides 8 channels with 24-bit resolution and programmable gain. Signal preprocessing includes high-pass filtering to reduce baseline wandering and DC offset adjustment. A voltage selector allows powering active electrodes for capacitive sensing.

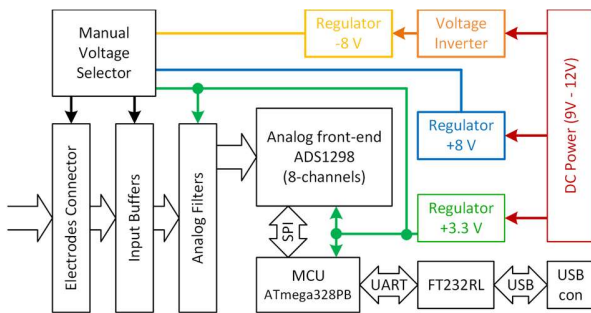


Figure 1. The principal block diagram of developed bioamplifier.

The compact device connects to electrodes via audio jack adapters and interfaces with a PC through USB. A MATLAB/C# client application enables parameter configuration, data acquisition control, and real-time signal display.

III. RESULTS

System performance was validated by comparing ECG measurements against a gold-standard Biopac MP36 device,

yielding a correlation coefficient of 0.968. Power spectral density analysis showed close agreement between the signals.

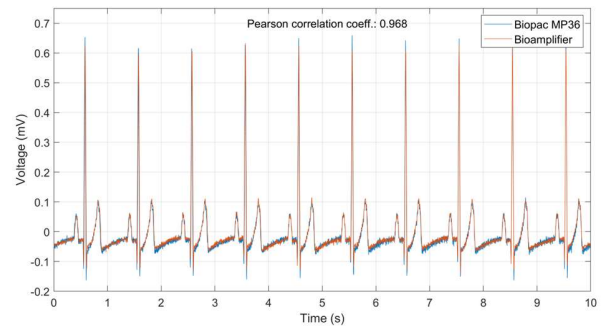


Figure 2. A representative example of the one-lead ECG measured from patient simulator using the developed bioamplifier and Biopac MP36.

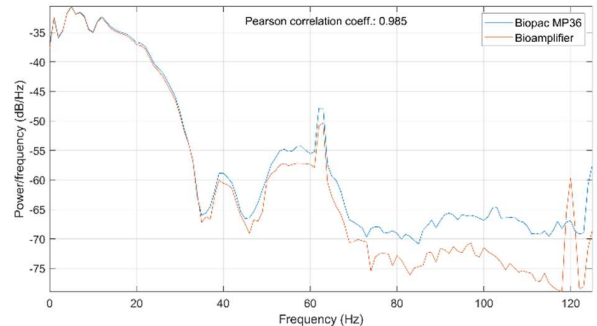


Figure 3. Power spectral density of the one-lead ECG measured from patient simulator using the developed bioamplifier and Biopac MP36.

IV. DISCUSSION & CONCLUSION

The low-cost, multi-modal design makes this bioamplifier suitable for both research and clinical applications, particularly in resource-constrained settings. Its flexibility enables use with various electrode types and biopotential signals. Future work will focus on further miniaturization and integration with wearable devices.

This bioamplifier advances biosignal acquisition technology by providing an accessible, versatile platform for high-quality biopotential measurements across multiple sensing modalities. Its modular design and configurability make it a valuable tool for biomedical research and development of novel biosensing applications.

Determination of operational parameters of an asynchronous electric drive with sequential reactive power compensation

Vasyl Malyar
Institute of Power Engineering and
Control Systems
Lviv Polytechnic National University
Lviv, Ukraine
vasyl.s.maliar@lpnu.ua

Orest Hamola
Institute of Power Engineering and
Control Systems
Lviv Polytechnic National University
Lviv, Ukraine
orest.y.hamola@lpnu.ua

Volodymyr Maday
Institute of Power Engineering and
Control Systems
Lviv Polytechnic National University
Lviv, Ukraine
volodymyr.s.maday@lpnu.ua

Ivanna Vasylychshyn
Institute of Power Engineering and
Control Systems
Lviv Polytechnic National University
Lviv, Ukraine
ivanna.i.vasylychshyn@lpnu.ua

Abstract— Mathematical models and algorithms for calculating the characteristics and parameters of an electric drive based on an asynchronous motor with series-connected capacitors have been developed, enabling their parameter computation and determination of limit values under automatic control. The motor model accounts for magnetic core saturation and the effect of current displacement in rotor bars.

Keywords—asynchronous motor, reactive power, mathematical modeling, magnetic circuit saturation phenomenon, skin effect

I. INTRODUCTION

Asynchronous motors (AM) are the most common in modern electric drives. At the same time, they are the main consumers of reactive power, accounting for about 70%. The solution to the problem of high-quality power supply in distribution networks is based both on the use of modern electrical equipment and on ensuring the required power flows through compensation and regulation. The article discusses an individual circuit in which capacitors are connected directly to the motor terminals. Its advantage is that reactive power is not transmitted along the line but is generated at the point of consumption, which relieves the line of reactive currents and prevents voltage drops at the motor terminals.

II. MODEL DESCRIPTION

The purpose of the article is the development of a mathematical model to determine the permissible limit values of changes in the operating parameters of an electric drive system based on a squirrel-cage rotor AM with capacitive reactive power compensation.

Electromagnetic processes in AD with capacitors of capacity C connected in series in orthogonal coordinates x, y are described by a system of electrical equilibrium equations for the stator and rotor circuits.

$$\frac{d\psi_{sx}}{dt} = \omega_0 \psi_{sy} - r_s i_{sx} - u_{cx} + u_{sx},$$

$$\frac{d\psi_{sy}}{dt} = -\omega_0 \psi_{sx} - r_s i_{sy} - u_{cy} + u_{sy},$$

$$\frac{d\psi_{jx}}{dt} = (\omega_0 - \omega) \psi_{jy} - r_r i_{jx},$$

$$\frac{d\psi_{jy}}{dt} = -(\omega_0 - \omega) \psi_{jx} - r_r i_{jy}, \quad (j = 1, \dots, n), \quad (1)$$

where $u_{cx} = x_c i_{sy}$; $u_{cy} = -x_c i_{sx}$.

Below are examples of the results of calculating some motor characteristics ($P=15$ kW, $U=220$ V, $I_n=29.9$ A, $p_0=2$, $s_n=0.02$, $m_n=2.0$, $m_k=2.2$, $m_m=1.6$).

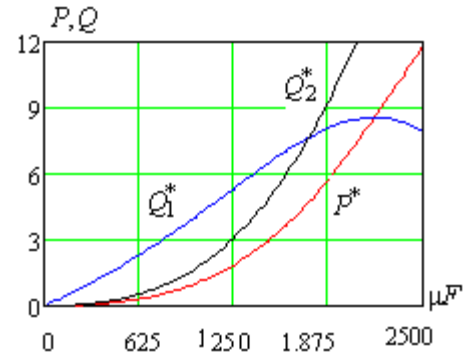


Fig. 1. Capacitor capacitance dependence of active power (P^*) and reactive power: at the system input (Q_1^*), at the motor stator (Q_2^*)

III. CONCLUSION

The article develops a mathematical model for analyzing the operation of an electric drive system based on a squirrel-cage motor with capacitive reactive power compensation and determining the permissible limits of changes in operating parameters.

- [1] M.H. Popovych, O.Yu. Lozynskyy, V.B. Klepikov, Electromechanical automatic control systems and electric drives, Kyiv: Lybid, 2005.
- [2] Klyuyev O.V., Sadovoy O.V., Optimization of energy characteristics of an asynchronous valve cascade, Collection of scientific papers DSTU, issue 1(28), pp.73–81, 2016.

Dynamic Response of Energy System under Contingency: A Simulation-Based Assessment

Zagkhorol Bayasgalan
Power Engineering School
Mongolian University of Science and Technology
Ulaanbaatar, Mongolia
zagdkhorol@must.edu.mn

Munkh-Erdene Oyundelger
National Dispatching Center
Mongolian University of Science and Technology
Ulaanbaatar, Mongolia
o.munkheredene1215@gmail.com

Nomin Lkhgvasuren
SCADA Engineer of MCS International
Mongolian University of Science and Technology
Ulaanbaatar, Mongolia
nomin.l@mcsi.mn

Tsetsgee Bayasgalan
School of Management
Mongolian University of Science and Technology
Ulaanbaatar, Mongolia
btsetsgee@must.edu.mn

Abstract— This study investigates the dynamic behavior of Mongolia's Western Energy System (WES) under contingency scenarios through simulation-based analysis. WES faces notable reliability concerns due to its heavy reliance on electricity imports and structural weaknesses in key infrastructure, particularly the Bayn-Ulgii substation. To address these challenges, a 30 MW thermal power plant was proposed and modeled for parallel connection at the 110 kV bus of the Bayn-Ulgii substation. Using DigSILENT PowerFactory, load flow and dynamic stability simulations were performed under both low-load summer and peak-load winter conditions. A critical fault case—a two-phase short circuit on a major transmission line—was used to test the system's ability to maintain synchronism during disturbances. The results show that integrating local generation helped raise voltage levels by up to 7.4 kV and maintained system stability throughout the event. These findings suggest that strategically placed local generation can significantly improve voltage support, ease transmission loading, and enhance overall system resilience under stress.

Keywords— *power system stability, contingency analysis, local generation, voltage support, grid reliability, parallel integration*

Electrical Engineering in Wartime: Perspectives on Ukraine's Energy Sector

Oksana Hoholyuk
*Institute of Power Engineering and
Control Systems*
Lviv Polytechnic National
University
Lviv, Ukraine
oksana.p.hoholyuk@lpnu.ua

Iryna Moroz
*Institute of Power Engineering and
Control Systems*
Lviv Polytechnic National
University
Lviv, Ukraine
iryna.y.moroz@lpnu.ua

Ivanna Vasylychshyn
*Institute of Power Engineering and
Control Systems*
Lviv Polytechnic National
University
Lviv, Ukraine
ivanna.i.vasylychshyn@lpnu.ua

Myroslav Sabat
*Institute of Power Engineering and
Control Systems*
Lviv Polytechnic National
University
Lviv, Ukraine
myroslav.b.sabat@lpnu.ua

Abstract— This article addresses the challenges faced by the energy sector due to military actions and their impact on the educational process in higher education institutions, particularly in the teaching of electrical engineering. The importance of developing engineering education as a key factor for the sustainable recovery of Ukraine's energy sector is emphasized.

Keywords— energy infrastructure, energy security, restoration of energy systems, electrical engineering education

Introduction

The full-scale invasion of Ukraine by the Russian Federation began on February 24, 2022; however, the conflict effectively started in 2014 with the annexation of Crimea and parts of the Donbas region. Military operations have resulted in hundreds of thousands of military casualties on both sides, along with tens of thousands of civilian deaths.

As of 2024, Russia occupies approximately 20% of Ukraine's territory. The war has triggered a large-scale humanitarian crisis: more than 8 million Ukrainians have become internally displaced, and over 8.2 million have been forced to flee the country (as of April 2023). This constitutes the largest refugee crisis in Europe since World War II. The paper aims to analyze the current state of Ukraine's energy infrastructure under martial law and to develop methodologies for teaching electrical engineering disciplines in higher education institutions.

I. DESCRIPTION

The full-scale war that has continued since 2022 has caused immense hardship for the Ukrainian population, severely affecting critical infrastructure, the energy sector, the economy, and overall social stability. Military actions have caused extensive damage to residential areas, industrial facilities, transportation hubs, and energy systems. Repeated shelling and airstrikes targeting energy infrastructure have resulted in frequent power outages, disrupting the operations of businesses, educational institutions, and public services.

This instability has led to mass population displacement, widespread job losses, and a decline in living standards. Tens of thousands of people have lost their homes, and millions have become internally displaced or have been forced to leave the country, placing extraordinary pressure on social services and governance systems.

Beyond physical destruction, the war has severely destabilized Ukraine's education, healthcare, and vocational training systems, hampering the normal functioning of

society. In this context, efforts to adapt infrastructure, support internally displaced persons, ensure energy security, and maintain educational continuity are especially critical.

This article examines damaged infrastructure that requires full or partial restoration and proposes a strategic approach to rebuilding and modernizing Ukraine's energy sector.

It also addresses the challenges faced by higher and specialized technical education institutions in teaching electrical engineering disciplines during wartime. The content and scope of core and supplementary subjects are reviewed, with a focus on preparing students to operate electrical systems under emergency conditions. A list of recommended electrical engineering and computer-based disciplines is presented to support this goal.

II. THE ROLE OF ELECTRICAL ENGINEERING EDUCATION

The article places particular emphasis on the challenges of teaching electrical engineering in higher and specialized technical institutions during wartime. Damage to infrastructure, frequent power outages, disruptions to internet access, and the need to integrate internally displaced students all necessitate the rapid adaptation of curricula and teaching methods. To meet these challenges, the following measures are proposed:

- Updating course content to include topics on energy resilience, autonomous power systems, and emergency management of energy networks.
- Incorporating computer modeling and simulation tools to facilitate remote learning in electrical engineering.

In addition, the article discusses the broader difficulties of teaching during wartime and emergency situations, and the need for educators to continually adapt to changing conditions from both didactic and scientific-technical perspectives.

REFERENCES

- [1] Ministry of Energy of Ukraine. Status of Ukraine's Energy System under Martial Law [Electronic resource]. – Available at: <https://mev.gov.ua>
- [2] NEC "Ukrenergo". Daily Operational Reports on the State of the Energy System [Electronic resource]. – Available at: <https://ua.energy>
- [3] International Energy Agency. Ukraine Energy Profile 2023 [Electronic resource]. – Available at: <https://www.iea.org/reports/ukraine-energy-profile>

Enhancing Insulator Inspection: A YOLO and DETR Approach to Image-Based Defect Detection

1st Dominika Pacek
Faculty of Electrical Engineering
Warsaw University of Technology
Warsaw, Poland
dominpacek@gmail.com

2nd Zuzanna Krawczyk-Borysiak
Faculty of Electrical Engineering
Warsaw University of Technology
Warsaw, Poland
zuzanna.krawczyk@pw.edu.pl

Abstract—This paper addresses automatic defect detection in electrical insulators from photographs using two deep learning models: You Only Look Once (YOLO) and Detection Transformer (DETR). The study evaluates models that can be trained and tested on consumer-grade hardware, using the Insulator Defect Image Dataset (IDID). Results show that deep learning provides an effective solution for this task, with YOLOv9s achieving the highest performance (95.1% F1 score on the test set).

Index Terms—YOLO, DETR, insulators defects, object detection, transformers

I. INTRODUCTION

High-voltage insulators, made of non-conductive materials, are critical components of electrical power systems. Their primary role is to mechanically support and electrically isolate conductors while preventing undesired current flow. Prolonged exposure to environmental and operational stresses often leads to defects such as surface contamination, flashover damage, physical breakage, and erosion. [2] These faults are among the main causes of power system failures, making timely and accurate defect localization essential. Traditionally, inspection relay on manual human assessment, which is time-consuming. An alternative can be automated image-based diagnostics, enabled by aerial inspection platforms or inspection robots and advanced computer vision algorithms [3], [4].

The main objective of this paper is to assess the usefulness of two deep learning model architectures: You Only Look Once (YOLO) and Detection Transformer (DETR) in insulator inspection applications. In addition, the authors focus on smaller models that are less costly to train and deploy, making them accessible to institutions without high-performance infrastructure.

II. TRAINING AND RESULTS

The dataset used for training and evaluation models was Insulator Defect Image Dataset (IDID) [1], version 1.2 released by Electric Power Research Institute (EPRI). The set consists of high quality images of transmission line insulators with annotations of whole insulator string and three shell subclasses: flashover damage, broken and good. The initial data set was split into separate train (1278 images), validation (324) and test (88) data sets prior to training.

In the initial training phase, a broad set of YOLO models (versions 3 through 11, including n, small, and tiny variants) were trained for 100 epochs, starting from pre-trained weights. Among them, YOLOv9s achieved the best results and was selected for further experimentation. The DETR model was fine-tuned under four different configurations, varying learning rate, input image size, and max-grad-norm parameters. The most promising configuration was then selected for extended training. Finally, the three best-performing models were trained for 250 epochs, with results summarized in Figure 1. YOLOv9s outperformed all DETR configurations, achieving mAP50 scores of 0.993 and 0.864 on the validation and test sets, respectively, compared to 0.750 and 0.864 for the best DETR model.

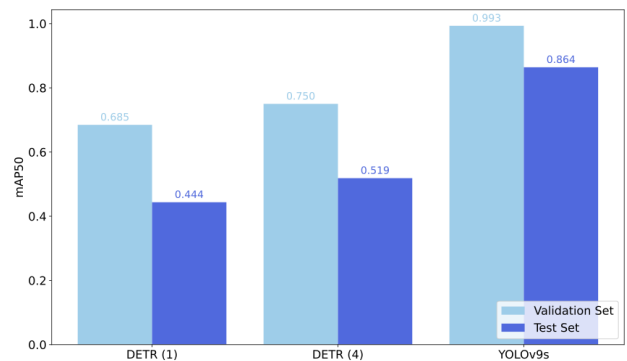


Fig. 1. mAP50 of the models in the 250th epoch on validation and test sets. DETR(1) – model trained on images with lower resolution (320x320), DETR(4) – model trained on images with resolution 480x480

REFERENCES

- [1] Lewis D., Kulkarni P., "Insulator Defect Detection", IEEE Dataport, August 11, 2021, doi:10.21227/vkdw-x769
- [2] Kiessling F., Nefzger P., Nolasco J.F., Kaintzyk U., Overhead power lines: planning, design, construction, Springer, 2014
- [3] Alhassan A.B., Zhang X., Shen H., Xu H., Power transmission line inspection robots: A review, trends and challenges for future research, International Journal of Electrical Power & Energy Systems, vol. 118, 2020
- [4] Wang Z., Gao Q., Xu J., Li D., A review of UAV power line inspection in Advances in Guidance, Navigation and Control: Proceedings of 2020 International Conference on Guidance, Navigation and Control, ICGNC 2020, Tianjin, China, October 23–25, 2020

Epileptic Seizure Detection from EEG Signals Using a Subject-Dependent Approach

Kamil Grzegorzewski

*Institute of Theory of Electrical
Engineering, Measurements and
Information Systems*

*Warsaw University of Technology
Warsaw, Poland*

kamil.grzegorzewski.stud@pw.edu.pl

Andrzej Majkowski

*Institute of Theory of Electrical
Engineering, Measurements and
Information Systems*

*Warsaw University of Technology
Warsaw, Poland*

andrzej.majkowski@pw.edu.pl

Marcin Kołodziej

*Institute of Theory of Electrical
Engineering, Measurements and
Information Systems*

*Warsaw University of Technology
Warsaw, Poland*

marcin.kolodziej@pw.edu.pl

Abstract— The article presents research on epileptic seizure detection using the CHB-MIT Database. The aim of the study was to determine whether there are common, universal features that enable accurate seizure detection for all 23 subjects. The analysis showed that no universal set of features is effective for every individual. However, effective seizure detection is possible using classifiers trained separately for each subject (subject-dependent). Feature extraction and selection from the EEG signals were performed, followed by classification using three models: k-NN, SVM, and Random Forest. The average values for sensitivity, precision, and F1-score range from 80% to 46%, 61% to 42%, and 55% to 48%, respectively.

Keywords— EEG, epilepsy, electroencephalography, SVM, KNN, Random Forest

I. INTRODUCTION

Epilepsy is one of the most common neurological disorders, affecting approximately 50 million people worldwide [1]. The automation of seizure detection using artificial intelligence methods, especially machine learning, offers new opportunities for diagnosis and patient monitoring [2]. A major challenge is the high variability of EEG signals, both between different patients and within the same patient, which makes it difficult to develop universal algorithms. Additionally, seizure samples represent only a small fraction of all EEG data, and effective detection requires model personalization due to individual differences. The aim of this research is to develop an efficient method for automatic seizure detection from EEG signals using machine learning techniques.

II. MATERIALS AND METHODS

This study utilized data from the CHB-MIT Scalp EEG Database, which contains long-duration, meticulously annotated EEG recordings ideal for research on automatic seizure detection. The dataset includes EEG signals sampled at 256 Hz, collected from 23 pediatric patients monitored at a Boston hospital during the diagnosis and treatment of drug-resistant epilepsy. In total, the database comprises 664 EEG files, each lasting between 1 and 4 hours and containing 23 channels recorded using the 10-20 electrode system, with each patient contributing between 9 and 42 files.

Initially, the EEG signals underwent preprocessing, including noise filtering (using a 60 Hz notch filter and a high-pass filter) and segmentation into non-overlapping 2-second windows. For each channel and window, an extensive set of features was extracted in three domains: time (geometric mean, kurtosis, mean, skewness), frequency (power in the alpha, beta, delta, gamma, and theta bands), and time-

frequency, using a 5-level Daubechies wavelet transform. Feature importance was then analyzed separately for each patient to identify key EEG parameters relevant for accurate seizure detection. Statistical tests based on t-statistics were used to compare feature values between seizure and non-seizure segments. The results confirm that the set of most significant features varies from patient to patient, supporting the subject-dependent approach.

Subsequently, the features for each patient were used to train KNN, SVM, and Random Forest models to distinguish seizure states from normal brain activity. The data was split into training and test sets in a 50:50 ratio, ensuring balanced classes. Each model was trained and tested individually for every patient.

III. RESULTS

The classification results for the SVM (linear kernel), KNN, and Random Forest (RFC) models are presented in Table I. These are average values calculated across all patients.

TABLE I. CLASSIFICATION RESULTS

Model	Precision (%)	Sensitivity (%)	F1 (%)
KNN	79.53	41.95	49.53
Random Forest	77.78	47.00	54.70
SVM	46.42	61.42	48.45

The KNN model achieved good results, with an average precision of 79.53%, sensitivity of 41.95%, and an F1-Score of 49.53%. Random Forest demonstrated slightly lower precision (77.78%) but achieved the highest F1-Score among the tested models—54.70%—while also providing stable performance. SVM obtained the highest sensitivity (61.42%), but its precision (46.42%) and F1-Score (48.45%) were the lowest. These results confirm the effectiveness of the proposed methods for seizure detection. However, it is important to note that model performance varies significantly between patients, due to individual EEG characteristics and the diverse manifestations of seizures. Each patient represents a unique case, presenting distinct classification challenges.

REFERENCES

- [1] S. J. M. Smith, „EEG in the diagnosis, classification, and management of patients with epilepsy”, *J. Neurol. Neurosurg. Psychiatry*, t. 76 Suppl 2, nr Suppl 2, s. ii2-7, cze. 2005, doi: 10.1136/jnnp.2005.069245.
- [2] A. T. Tzallas *i in.*, „Automated Epileptic Seizure Detection Methods: A Review Study”, w *Epilepsy - Histological, Electroencephalographic and Psychological Aspects*, IntechOpen, 2012. doi: 10.5772/31597.

Evaluating the Effect of Tattoos on Photoplethysmography Imaging Perfusion Monitoring

Author: Michal Labuda

Co-authors: Patrik Durajka; Jan Seleng; Veronika Wohlmuthova

University of Zilina, Faculty of Electrical Engineering and Information Technology, Department of Electromagnetic and Biomedical Engineering, Univerzitna 8215/1, Zilina 010 26, Slovakia

Corresponding Author: michal.labuda@uniza.sk

This study is focused on investigating the impact of tattoos on the evaluation of skin perfusion using photoplethysmography imaging (PPGI), a non-contact optical method for monitoring changes in blood volume in the skin. Cardiac activity causes variations in blood volume within the observed area, altering the skin's optical properties—specifically the absorption of light by hemoglobin—which in turn generates the PPGI signal. The PPGI signal is also influenced by the skin's reflectance and light scattering. The PPGI signal consists of an pulsatile (AC) component, related to cardiac activity and respiration, and a non-pulsatile (DC) component, representing bloodless tissue and bones. PPGI is based on the same principle as classical PPG (photoplethysmography), but instead of a single-point sensor, it uses a camera that captures the entire skin area. This enables spatial monitoring of perfusion changes and the creation of perfusion maps. The basic components of a PPGI measurement setup include a camera and an illumination device operating at a selected wavelength or light spectrum [1], [2].

In the material and methods, a measurement setup is designed and implemented, consisting of a laptop, an RGB camera, an LED light source, and a BIOPAC MP36 system with a PPG sensor for recording a reference signal. Measurements were conducted on two subjects with forearm tattoos. Four regions of interest were analyzed: tattooed and non-tattooed skin, each with and without the application of a vasodilating (warming) gel. Data were processed in MATLAB in two frequency bands (heart rate [HR] and DC), with perfusion maps and time signals created and analyzed, supplemented by tables of mean and root-mean-square values.

The processing involved spectral analysis of the individual perfusion maps, as well as monitoring signal changes over short time intervals within defined regions of interest, enabling a more detailed evaluation of local blood supply variations. The results were supplemented with tables containing mean and root mean square (RMS) values, providing a quantitative overview of signal behavior in the studied areas. Perfusion maps were generated for each of the RGB color channels, representing the intensity of both the pulsatile (AC) and non-pulsatile (DC) components of the signal. Each map was constructed from four time segments. The purpose of this temporal segmentation was to capture the progression and dynamics of perfusion changes in response to the application of a vasodilating gel—from the initial moment of its effect to the later phase of its influence. This approach enabled analysis of the temporal development of hemodynamic changes and allowed comparison of responses across different spectral regions of light.

The results demonstrating that the presence of tattoos significantly affects the quality of the PPGI signal. Tattooed areas exhibited increased noise and reduced signal amplitude due to higher light absorption by pigments in the skin. This effect was observed in both the HR and DC bands, indicating potential distortion in the assessment of both rapid and slow perfusion changes. While the application of a vasodilating gel enhanced perfusion overall, pronounced differences between tattooed and non-tattooed regions persisted. An intriguing observation was a small area containing white pigment, which showed different reflective properties and influenced the PPGI signal differently than darker pigments. Elevated values in this area suggest that lighter pigments increase light reflectance compared to darker pigments, which absorb more light—a factor that must be considered in signal interpretation.

The findings confirm that PPGI is a sensitive and effective method for monitoring perfusion changes in non-tattooed skin. However, the presence of tattoos substantially degrades signal quality and may lead to misinterpretation. Therefore, tattoo pigments should be recognized as potential confounding factors in clinical or research use of PPGI. These results also open opportunities for future research aimed at optimizing PPGI for use on tattooed skin, such as employing alternative light wavelengths or advanced algorithms to compensate for optical attenuation.

- [1] S. Borik, S. Lyra, M. Paul, C. H. Antink, S. Leonhardt, and V. Blazek, "Photoplethysmography imaging: camera performance evaluation by means of an optoelectronic skin perfusion phantom," *Physiol. Meas.*, vol. 41, no. 5, p. 54001, 2020.
- [2] P. A. Kyriacou and J. Allen, *Photoplethysmography: Technology, Signal Analysis and Applications*. Academic Press, 2021.

Evaluation of selected missing data imputation methods

1st Jakub Jasiński
Faculty of Electrical Engineering
Warsaw University of Technology
Warsaw, Poland
jakub.jasinski2.stud@pw.edu.pl

2nd Robert Szmurło
Faculty of Electrical Engineering
Warsaw University of Technology
Warsaw, Poland
robert.szmurlo@pw.edu.pl

3th Krzysztof Siwek
Faculty of Electrical Engineering
Warsaw University of Technology
Warsaw, Poland
krzysztof.siwek@pw.edu.pl

Abstract—Missing values are common in time-series data and degrade analysis and ML performance. This study characterizes missingness patterns and benchmarks imputation methods, from simple statistics to regression, MLPs, and LSTMs, on air-pollution series (PM₁₀, PM_{2.5}). We evaluate accuracy and thus impact on downstream forecasting. The results show that the best-performing models are the LSTM models; less accurate but faster alternatives seem to be regression and MLP, while the mean imputation achieves the highest error values.

Index Terms—missing data, data imputation, time series, regression, LSTM, atmospheric pollution, PM10, PM2.5

I. PROBLEM STATEMENT

Air pollution is widely recognized as one of the leading threats to both environmental stability and public health today. Air-quality monitoring time series frequently contain missing values, absent or unrecorded observations at specific time-stamps, that disrupt the continuity and integrity of temporal analyses. These gaps can arise from sensor failures, transmission errors, irregular sampling, calibration or maintenance downtime, and other operational issues. Missing data pose substantial challenges for forecasting, modeling, and anomaly detection [1]. Predictive models for air quality and climate heavily depend on consistent data, and missing values can reduce their accuracy and reliability.

In the presented research the following imputations methods were investigated: mean imputation, regression (iterative imputer with Bayesian Ridge for regression estimates), Neural networks (a Multi-Layer Perceptron (MLP) involving framing the problem as a supervised learning task with use of a sliding window to transform sequences of past observations into input features), LSTM recurrent deep network (sequence-to-sequence strategy).

The GIOS Air Quality Archive [2] database of air pollution measurements has been used. Two key pollutants of health and environmental concern which were investigated in this research: PM₁₀ (Particulate Matter ≤ 10 micrometres) and PM_{2.5} (Particulate Matter ≤ 2.5 micrometres). During data exploration task an analysis was carried out to identify how much data is missing in the dataset.

II. RESULTS

To check the accuracy of the previously mentioned methods, randomly selected values from the available time series have

been marked as artificially missing when using an imputation method. Then, the new values will be validated with metrics: SMAPE, MAE, and RMSE.

TABLE I
PERFORMANCE METRICS FOR PM₁₀ AND PM_{2.5} AND 0.5% MISSING DATA

Model	PM ₁₀			PM _{2.5}		
	SMAPE (%)	MAE ($\mu\text{g}/\text{m}^3$)	RMSE ($\mu\text{g}/\text{m}^3$)	SMAPE (%)	MAE ($\mu\text{g}/\text{m}^3$)	RMSE ($\mu\text{g}/\text{m}^3$)
Mean	31.93	5.52	9.12	32.10	4.50	7.24
Reg	20.81	3.05	4.78	15.77	2.37	5.63
MLP	19.07	2.78	3.75	16.31	2.15	4.20
LSTM	9.88	2.09	2.83	9.06	1.95	2.60

The LSTM model yields the most accurate predictions across all metrics for both pollutants and both missing data ratios. This demonstrates the model's capability to effectively utilize recent temporal context for short-gap and medium-gap recovery, outperforming statistical approaches.

III. CONCLUSIONS

The article presents and compares several approaches to imputing missing PM₁₀ and PM_{2.5} values in air-quality time series. A key contribution is the identification of the most efficient approach for imputing data. An extra output is characterization of missingness, its frequency, gap length, and volume, and a systematic evaluation under two different missing-data scenarios.

The experiments show that LSTM models consistently perform best, especially under moderate to severe missingness. By learning temporal dependencies, LSTM achieves the lowest errors across most conditions, supporting their suitability for quality of air (QOA) time-series imputation.

REFERENCES

- [1] I. Pratama and et al., "A review of missing values handling methods on time-series data," in *2020 3rd International Conference on Information and Communications Technology (ICOIACT)*, IEEE, 2020, pp. 286–291. DOI: 10.1109/ICOIACT50329.2020.9332008.
- [2] Chief Inspectorate of Environmental Protection, *Air quality measurement data archive*, <https://powietrze.gios.gov.pl/pjp/archives>, Accessed: 2025-04-02.

Evaluation of Specific Absorption Rate in Ear Tissue After Exposure to Electromagnetic Fields from Cell Phone

Zuzana Psenakova
Department of electromagnetics and
biomedical engineering
Faculty of electrical engineering and
information technology
University of Zilina
Zilina, Slovakia
zuzana.psenakova@uniza.sk

Nevedel Jozef
Department of electromagnetics and
biomedical engineering
Faculty of electrical engineering and
information technology
University of Zilina
Zilina, Slovakia
nevedel2@stud.uniza.sk

Milan Smetana
Department of electromagnetics and
biomedical engineering
Faculty of electrical engineering and
information technology
University of Zilina
Zilina, Slovakia
milan.smetana@uniza.sk

Daniela Gombarska
Secondary Vocational School of Electrical
Engineering
Zilina, Slovakia
gombarskad@soseza.sk

Abstract— This study presents a comprehensive simulation-based analysis of the effects of electromagnetic (EM) fields generated by mobile phones on human ear tissue, focusing on the distribution of specific absorption rate (SAR) and its frequency-dependent behavior. The motivation behind this work stems from growing public concern about long-term exposure to EM radiation from handheld wireless devices and their potential biological effects, particularly on anatomically sensitive and frequently exposed regions, such as the ear. To evaluate these effects, an anatomically detailed three-dimensional (3D) model of the human ear was created, encompassing key structures including the auricle, external auditory canal, tympanic membrane, auditory ossicles (malleus, incus, stapes), and cochlea. The model was imported into CST Studio Suite, a specialized electromagnetic simulation environment based on the finite integration technique (FIT). A set of microstrip patch antennas, each designed to resonate at commonly used communication frequencies—1800 MHz, 2.4 GHz, and 5 GHz—was positioned near the auricle to emulate real-world mobile phone usage conditions. Electromagnetic field simulations were performed to determine the spatial distribution of SAR across ear tissues under controlled input power conditions. Material properties such as dielectric permittivity, conductivity, and tissue density were assigned to each anatomical component based on validated biomedical databases. The simulations accounted for complex tissue heterogeneity, geometrical intricacies, and near-field interactions to capture realistic absorption dynamics.

To further analyze age-related exposure differences, two voxel-based full-body anatomical models—HUGO (adult male) and Child (pre-adolescent body)—were incorporated into the simulations. This allowed for the comparison of SAR levels between different body sizes and tissue compositions, which are known to influence electromagnetic field penetration and energy absorption. Antennas were again placed near the ear in both models, and SAR distributions were calculated for each frequency band under a standardized input power of 1 W.

The results demonstrate that both frequency and anatomical structure significantly influence SAR levels. Higher frequencies, such as 5 GHz, exhibit stronger surface absorption with localized SAR peaks in the auricle and outer ear canal. Lower frequencies, such as 1800 MHz, tend to penetrate more deeply into the tissue, affecting the middle and inner ear structures. The voxel-based simulations revealed that the Child model experienced higher SAR values than the adult HUGO model, primarily due to thinner skull bones and smaller anatomical dimensions, resulting in lower attenuation of the incident field.

All simulated SAR values were compared with the International Commission on Non-Ionizing Radiation Protection (ICNIRP) 2020 safety thresholds, confirming compliance for the evaluated scenarios. The simulations also enabled the visualization of electric field distribution, highlighting areas of energy concentration and potential risk. This level of detail provides essential insights for mobile device manufacturers, such as the need to consider frequency and anatomical structure in device design, as well as for regulatory bodies, who can use the findings to update safety standards and guidelines for device certification and public safety.

In conclusion, this simulation-driven study underscores the importance of considering frequency, device placement, and user anatomy when evaluating EM field exposure from mobile phones. The findings of this study, particularly the influence of frequency and anatomical structure on SAR levels can guide mobile device manufacturers in designing safer devices and regulatory bodies in setting more effective safety standards. Numerical modelling proves to be a powerful tool for predicting SAR behavior in complex biological environments, paving the way for more accurate exposure assessments and improved guidelines for safe mobile device usage.

Keywords—Electromagnetic field (EMF), Specific absorption rate SAR, CST Studio Suite, voxel model (a three-dimensional representation of the human body used in simulations), human ear, patch antenna, ICNIRP, thermal effect

Experimental Study of Extremely Low Frequency and Static Magnetic Fields in Household Devices Using a Cost-Effective Portable Magnetometer

Author: Veronika Wohlmuthova

Co-authors: Michal Labuda; Lubomir Trpis; Mariana Benova;

University of Zilina, Faculty of Electrical Engineering and Information Technology, Department of Electromagnetic and Biomedical Engineering, Univerzitna 8215/1, Zilina 010 26, Slovakia

Corresponding Author: wohlmuthova@stud.uniza.sk

Electromagnetic fields (EMF) have become an inseparable part of modern life, generated by various household devices. Among the different EMF ranges, extremely low frequency (ELF) fields (≤ 300 Hz) [1] and static magnetic fields (DC) are also included. In household environments, ELF magnetic fields are most commonly generated by devices powered by alternating current at 50 Hz, such as hair dryers, irons, refrigerators, or washing machines. Together with DC magnetic fields, these sources create magnetic fields whose intensity and frequency characteristics may vary depending on the type of device, distance from the source, and operational mode [2].

Despite their low energy, prolonged exposure to these fields has raised scientific and public concerns, leading to increasing interest in their potential health effects, particularly among vulnerable population groups such as children [3], [4] or individuals with implantable medical devices [5].

In response to these potential negative effects, exposure limit standards have been developed. For instance, the International Commission on Non-Ionizing Radiation Protection (ICNIRP) [6] has set public exposure limits for time-varying magnetic fields at $100 \mu\text{T}$. In the case of static magnetic fields, it is recommended that long-term exposure in the general population does not exceed 400 mT [7].

Based on these requirements, we conducted measurements on commonly used household devices. To carry out the measurements, a custom-designed measuring system was developed, based on the MC858 [8] sensor (Magnetic Sciences), which operates on the induction principle and features a sensitivity of $22 \text{ mV}/\mu\text{T}$. The system was designed with an emphasis on accuracy, portability, and low cost. The measurement range spans from $0.06 \mu\text{T}$ to $100 \mu\text{T}$ in the frequency range of 7 Hz to 230 Hz for ELF fields, and up to $\pm 4800 \mu\text{T}$ for DC magnetic fields. Static fields are measured using the MPU9250 [9] sensor, which is also part of our system. To calculate the magnitude of magnetic induction from the induced voltage output of the MC858 sensor, algorithms for frequency and time-domain data analysis (FFT, CWT, ICWT) were used.

The experimental measurements were divided into two parts. In the first part, small, typically portable electrical appliances commonly found in household environments were measured inside a Faraday cage. The purpose of this experiment was to record isolated EMF generated by a selected device or appliance. This approach enabled the analysis of electromagnetic field attenuation along all axes at different distances from the source. With an isolated AC-powered source, it was also possible to analyze the higher harmonic frequency components of the generated field (50 Hz and its harmonics).

Considering the fact that truly isolated EMF sources do not exist in real-world conditions, additional measurements were carried out on electrical appliances in typical household environments. The recorded data were analyzed in terms of magnetic flux density, with two sensor-to-device distances monitored: directly at the power section of the appliance and at a typical user distance during device operation or use.

The measured magnetic induction values for both DC and ELF fields were compared to established exposure limit values.

These findings contribute to a more comprehensive understanding of the electromagnetic environment in households, highlighting the presence and variability of both ELF and DC magnetic fields generated by common appliances. This knowledge provides a valuable foundation for further research focused on detailed exposure assessment, health risk evaluation, and the development of safety recommendations - particularly for sensitive individuals such as children or people with implantable medical devices (e.g., pacemakers or neurostimulators), who may be more vulnerable to electromagnetic interference. It also supports public education initiatives aimed at promoting awareness and best practices in electromagnetic hygiene.

[1] J. Park, E. Jeong, and G. Seomun, 'Extremely Low-Frequency Magnetic Fields Exposure Measurement during Lessons in Elementary Schools', *Int. J. Environ. Res. Public Health*, vol. 17, no. 15, p. 5284, Jul. 2020, doi: 10.3390/ijerph17155284.

[2] A. A. Ponnle, 'Measurement and Assessment of Exposure to 50 Hz Magnetic Fields from Common Home Electrical Appliances', *Eur. J. Eng. Technol. Res.*, vol. 7, no. 3, pp. 119–127, Jun. 2022, doi: 10.24018/ejeng.2022.7.3.2832.

[3] G. Mezei, M. Gadallah, and L. Kheifets, 'Residential Magnetic Field Exposure and Childhood Brain Cancer: A Meta-Analysis', *Epidemiology*, vol. 19, no. 3, pp. 424–430, May 2008, doi: 10.1097/EDE.0b013e3181690715.

[4] M. Habash, P. Gogna, D. Krewski, and R. W. Y. Habash, 'Scoping Review of the Potential Health Effects of Exposure to Extremely Low-Frequency Electric and Magnetic Fields', *Crit. Rev. Biomed. Eng.*, vol. 47, no. 4, pp. 323–347, 2019, doi: 10.1615/CritRevBiomedEng.2019030211.

[5] L. Santini, G. B. Forleo, and M. Santini, 'Implantable devices in the electromagnetic environment', *J. Arrhythmia*, vol. 29, no. 6, pp. 325–333, Dec. 2013, doi: 10.1016/j.joa.2013.06.004.

[6] International Commission on Non-Ionizing Radiation Protection, 'GUIDELINES FOR LIMITING EXPOSURE TO TIME-VARYING ELECTRIC AND MAGNETIC FIELDS (1 Hz TO 100 kHz)'.

[7] 'GUIDELINES ON LIMITS OF EXPOSURE TO STATIC MAGNETIC FIELDS', *Health Phys.*, vol. 96, no. 4, pp. 504–514, Apr. 2009, doi: 10.1097/01.HP.0000343164.27920.4a.

[8] S. Magnetic, 'MC858 Sensor'. [Online]. Available: https://magneticsciences.com/mc858-sensor/?srsltid=AfmBOorqr17xi8udIB2R1KVEDSKnX9FMhKeg_BS98ifN-a5DIL_wcGPQ

[9] InvenSense, Inc., 'MPU-9250 Data Sheet – 9-Axis (Gyro + Accelerometer + Magnetometer) MEMS MotionTracking Device'. InvenSense, Inc., 2016. [Online]. Available: <https://invensense.tdk.com/wp-content/uploads/2015/02/PS-MPU-9250A-01-v1.1.pdf>

Explainability of Convolutional Neural Network: overview of methods

1st Magdalena Markowicz
Faculty of Electrical Engineering
Warsaw University of Technology
Warsaw, Poland
magdalena.markowicz.stud@pw.edu.pl

2nd Piotr Podgórski
Faculty of Electrical Engineering
Warsaw University of Technology
Warsaw, Poland
piotr.podgorski3.stud@pw.edu.pl

3rd Jan Kruszyński
Faculty of Electrical Engineering
Warsaw University of Technology
Warsaw, Poland
jan.kruszynski.stud@pw.edu.pl

4th Karim Sonbul
Faculty of Electrical Engineering
Warsaw University of Technology
Warsaw, Poland
karim.sonbul.stud@pw.edu.pl

5th Krzysztof Siwek
Faculty of Electrical Engineering
Warsaw University of Technology
Warsaw, Poland
krzysztof.siwek@pw.edu.pl

Abstract—Understanding and interpreting the decisions made by deep learning models has become an essential area of research in artificial intelligence. Convolutional neural networks (CNNs), despite their high performance in various tasks, often function as “black boxes,” making it challenging to explain their predictions. This study focuses on applying and evaluating different explainability techniques to CNN models to gain more insight into their decision-making processes. Using multiple approaches, our aim was to assess the effectiveness and reliability of these methods in improving the transparency and interpretability of neural networks.

Index Terms—XAI, Convolutional Neural Network, Explainability

I. INTRODUCTION

The field of Explainable Artificial Intelligence (XAI) has developed in response to the growing demand for greater clarity and interpretability in the outputs of complex machine learning models. Convolutional neural networks (CNNs), despite their widespread success, are frequently criticized for their lack of transparency in decision-making. XAI methodologies endeavour to pinpoint the input features that exert the greatest influence on a model’s predictions, typically through the application of gradient-based or perturbation-driven frameworks.

II. XAI METHODS USED IN THE STUDY

This study explores and compares four XAI methods applied to a CNN trained for binary image classification: LRP, LIME, Grad-CAM and DeepLIFT. Each method takes a different approach to relevance attribution. The goal of the research is to evaluate the effectiveness and reliability of these techniques in explaining CNN predictions. Visual and quantitative evaluations were performed using standardized metrics, aiming to identify the strengths and weaknesses of each method and their potential to enhance model transparency.

III. THE MODEL AND DATASET USED IN THE STUDY

For the study, we had used a preexisting CNN neural network for face recognition: with transfer learning technique.

The neural network used in this study was used with the classification of faces (with and without glasses on) in mind. We had picked the MeGlass due to its diversity of photos of faces with and without glasses. We used a subset of it (5 classes, ie photos of 5 different people with and without glasses) due to hardware constraints.

Before being passed through the model, the dataset was resized to 160x160, normalized, and split into training and validation subsets.

IV. CONCLUSION

Each method of XAI reflects a distinct paradigm of relevance attribution, utilising either backpropagation or local input perturbation to produce saliency maps that highlight features most influential in model predictions.

In terms of performance, Grad-CAM yielded the best results for IAUC (5.095) and DAUC (0.534), while LIME outperformed the other methods in DC (-0.203) and IIC (0.893). LRP achieved the top score for IC (0.118), and DeepLIFT performed best in AD (-0.223). However, DeepLIFT also demonstrated the weakest overall performance, recording the lowest values in three metrics: DAUC, DC, and IIC.

Overall, the findings highlight that while each XAI method offers distinct advantages, none proves universally superior across all evaluation criteria. Therefore, the choice of method should be guided by the specific interpretability needs of the application. In certain contexts, hybrid or ensemble approaches may provide more comprehensive and reliable insights into CNN decision-making processes.

Fast Adaptation to New Classes of Odors in the Electronic Nose

1st Krzysztof Siwek
Faculty of Electrical Engineering
Warsaw University of Technology
Warsaw, Poland
krzysztof.siwek@pw.edu.pl

2nd Tomasz Grzywacz
Faculty of Electrical Engineering
Warsaw University of Technology
Warsaw, Poland
tomasz.grzywacz@pw.edu.pl

3th Piotr Witkowski
Faculty of Electrical Engineering
Warsaw University of Technology
Warsaw, Poland
piotr.witkowski@pw.edu.pl

4th Tran Hoai Linh
School of Electrical and Electronic Engineering
Hanoi University of Science and Technology
Hanoi, Vietnam
linh.tranhoai@hust.edu.vn

Abstract—The rapid identification of novel odours in real-world environments remains a significant challenge for electronic nose (e-nose) systems. Traditional models rely on supervised learning with closed-set assumptions, limiting their effectiveness when encountering previously unseen odour classes. This paper proposes an artificial intelligence-driven framework that enables fast adaptation to new odour classes by combining open-set recognition, meta-learning, and reinforcement learning. The proposed system can autonomously detect unfamiliar scents, generalise from minimal examples, and strategically update its classification strategy without complete retraining. We outline the architecture, methodologies, and expected outcomes of our approach, providing a foundation for the next generation of intelligent, adaptive olfactory systems.

Index Terms—electronic nose, odour classification, open-set recognition

The electronic nose (e-nose) is an artificial olfactory system designed to detect, identify, and classify volatile compounds by mimicking the mammalian sense of smell. Over the past two decades, e-nose systems have gained significant attention in domains such as food quality monitoring, environmental control, industrial safety, and medical diagnostics. Despite their growing importance, current e-nose implementations largely rely on supervised learning techniques that assume a fixed set of odor classes known a priori. This assumption limits the scalability and robustness of such systems in real-world deployments, where previously unobserved and novel odors may emerge unexpectedly.

Recent advancements have highlighted the importance of reinforcement learning (RL) and active learning (AL) in developing autonomous and adaptive olfactory systems. Unlike traditional static methods trained once on fixed datasets, RL and AL enable the system to interactively adapt to the target domain. An RL agent can dynamically update its internal neural model by evaluating the outcomes of its actions, thus optimizing decision-making in uncertain or changing environments.

This capability is especially beneficial in electronic nose systems deployed under dynamic conditions, where novel or

unforeseen odor classes may arise.

Active learning further supports adaptation by allowing the system to selectively query the most informative samples for labeling, reducing the reliance on large annotated datasets. In olfactory classification, this means that the e-nose can request human input when an unusual or underrepresented signal is encountered, thereby improving sample efficiency. This is particularly useful when detecting rare diseases, failures in industrial installations, or other atypical odour events.

During the project, we propose an active learning algorithm that enables real-time system updates in response to newly acquired odor samples. This dynamic adaptation mechanism enhances the robustness of the system in the face of sensor drift, noise, and measurement uncertainty.

The adoption of RL and AL in e-nose platforms not only improves system performance but also introduces situational intelligence — enabling real-time decision-making and continuous adaptation without the need for full retraining. Continued research in this direction could pave the way for autonomous, self-optimizing sensor systems capable of learning and acting independently in real-time environments.

This work has explored the design of an adaptive electronic nose system capable of fast learning in open and unpredictable olfactory environments. By integrating techniques from open-set recognition, meta-learning, and reinforcement learning, we have proposed an architecture that addresses key limitations of traditional supervised e-nose models. The proposed approach enables the system not only to detect when a new class of odour is encountered, but also to adaptively learn it with minimal examples and intelligently decide when and how to request labels or update its model.

The application contexts considered throughout this paper, such as military threat detection, real-time industrial monitoring, and dynamic healthcare diagnostics emphasise the practical importance of fast, robust, and scalable adaptation.

Foreign Exchange Rate Forecasting Using Machine Learning Approaches: A Signal-Based Perspective

Konrad Maleńczak

*Department of Artificial Intelligence
Institute of Information Technology
Warsaw University of Life Sciences*

Nowoursynowska 159, 02-776 Warsaw, Poland

Artur Krupa

*Department of Artificial Intelligence
Institute of Information Technology
Warsaw University of Life Sciences*

Nowoursynowska 159, 02-776 Warsaw, Poland
artur_krupa@sggw.edu.pl / 0000-0001-8583-9873

Abstract—This paper uses machine learning techniques to present a signal-based approach to foreign exchange (FX) rate forecasting. Leveraging public data provided by the US Federal Reserve (G.5 monthly exchange rates), we treat FX rate fluctuations as discrete-time signals and investigate the application of recurrent neural networks (RNN), long-short-term memory (LSTM), and Prophet models for short-term prediction. The data set includes monthly exchange rates for major currencies such as the euro, yen and pound sterling over the last two decades. Pre-processing involves normalization and seasonal decomposition to improve model robustness. Our evaluation compares the accuracy of the model using RMSE and MAE metrics. Preliminary results suggest that LSTM networks may outperform classical time series models, particularly in capturing trend reversals and seasonal fluctuations; however, confirming this advantage requires further in-depth investigation, which constitutes the main objective of the present study. In addition to the core forecasting objective, we also analyze the structure of signal transformations induced by these models, emphasizing the role of memory gates and autoregressive behavior in learning currency dynamics. This work highlights the feasibility of applying signal processing and predictive machine learning techniques to economic time series data, contributing to interdisciplinary research at the intersection of signal engineering and financial analytics. By framing exchange rate forecasting as a signal interpretation problem, the study provides new insights into how temporal dependencies and periodicities can be algorithmically extracted and exploited for improved economic forecast accuracy.

Index Terms—foreign exchange, signal processing, time series forecasting, LSTM, machine learning, diagnostics

- [7] Y. Qu and X. Zhao, "Application of LSTM neural network in forecasting foreign exchange price," *J. Phys. Conf. Ser.*, vol. 1237, no. 4, Art. no. 042036, 2019. doi:10.1088/1742-6596/1237/4/042036.
- [8] H. Park, H. Lee, and M. Kim, "Prediction of Foreign Currency Exchange Rates Using an Attention-Based LSTM Model," *Mach. Learn. Appl.*, vol. 12, p. 100648, Apr. 2025. doi:10.1016/j.mlwa.2025.100648.
- [9] R. Bansal and J. Wei, "Predictive Modeling of Foreign Exchange Trading Signals Using Machine Learning Techniques," *Expert Syst. Appl.*, vol. 234, p. 121519, May 2025. doi:10.1016/j.eswa.2025.121519.
- [10] A. Izadyar, "Generative AI and Fundamentals-Based Exchange Rate Forecasting," SSRN preprint, Apr. 2025. doi:10.2139/ssrn.5228767.
- [11] S. Meng, Y. Zhang, and J. Wang, "Enhancing Exchange Rate Forecasting with Explainable Deep Learning Models," *arXiv preprint arXiv:2410.19241*, Oct. 2024. doi:10.48550/arXiv.2410.19241.
- [12] X. Shi, M. Liu, and Q. Zhou, "EUR/USD Exchange Rate Forecasting Incorporating Text Mining Based on Pre-trained Language Models and Deep Learning Methods," *arXiv preprint arXiv:2411.07560*, Nov. 2024. doi:10.48550/arXiv.2411.07560.

REFERENCES

- [1] S. Agarwal, S. Sharma, K. N. Faisal, and R. R. Sharma, "Time-Series Forecasting Using SVM-LSTM: A Hybrid Approach for Stock Market Prediction," *J. Probab. Stat.*, vol. 2025, Article ID 9464938, 2025. doi:10.1155/jpas/9464938.
- [2] S. J. Taylor and B. Letham, "Forecasting at scale," *PeerJ Preprints*, vol. 5, e3190v2, Sep. 2017. doi:10.7287/peerj.preprints.3190v2.
- [3] C. Tsuji, "Exchange rate forecasting via a machine learning approach," *iBusiness*, vol. 14, no. 3, pp. 119–126, 2022. doi:10.4236/ib.2022.143009.
- [4] L. G. Nielsen, "Machine learning for foreign exchange rate forecasting," M.S. thesis, Dept. of Mathematics, Imperial College London, London, UK, 2018. [Online].
- [5] X. Zhang, "Financial time series forecasting based on LSTM neural network optimized by wavelet denoising and whale optimization algorithm," *Academic Journal of Computing & Information Science*, vol. 5, no. 7, pp. 1–9, 2022. doi:10.25236/AJCIS.2022.050701.
- [6] R. Küçük, "Forecasting foreign exchange rate with machine learning techniques," M.S. thesis, Dept. of Statistics, Middle East Technical University, Ankara, Turkey, 2023. [Online].

Four types of short circuit currents in three-phase electrical networks

Jacek Korytkowski
Warsaw University of Technology,
Faculty of Electrical Engineering,
ul. Koszykowa 75,
00-662 Warszawa, Poland,
jacek.korytkowski@pw.edu.pl

Krzysztof Siwek
Warsaw University of Technology,
Faculty of Electrical Engineering,
ul. Koszykowa 75,
00-662 Warszawa, Poland,
krzysztof.siwek@pw.edu.pl
<https://orcid.org/0000-0003-2642-2319>

Kazimierz Mikołajuk
Warsaw University of Technology,
Faculty of Electrical Engineering,
ul. Koszykowa 75,
00-662 Warszawa, Poland,
kazimierz.mikolajuk@pw.edu.pl

Andrzej Toboła
Warsaw University of Technology,
Faculty of Electrical Engineering,
ul. Koszykowa 75,
00-662 Warszawa, Poland,
andrzej.tobola@pw.edu.pl

Abstract— The paper presents the analysis and method of short circuit current evaluation in three-phase electrical networks. The grid parameters are recognized by reactive current injection. The analytical and numerical results are presented. The numerical results prove the effectiveness of the proposed method.

Keywords— short circuit current, disturbance method, current prediction.

I. INTRODUCTION

The equivalent circuit parameters of a power supply system such as short circuit impedance are important data for both power supply authorities and industrial customers. The parameters have several applications. They are used to calculate the short circuit currents and to verify models of power system networks [1,2].

Several methods have been proposed to calculate the power system impedance parameters. They can be classified into two groups: invasive and noninvasive. The noninvasive approaches use the existing load current and voltage variations to identify the network equivalent impedance [1,2]. The invasive approaches impose intentional disturbances to the system and use the voltage and current response for estimation. These experiments can be oriented on the short-circuit current evaluation. One of such methods consists on short time short-circuit execution [3].

Estimation of a short-circuit current in electrical power systems is the important problem. Methods of such currents evaluation have been elaborated from the beginning of electrical grid development. The analysis of numerical grid models is one of the important approach for short-circuit current evaluation, this is valuable approach [4,5,6,7,8]. Numerical models comprise whole electrical systems and should be permanently bring up to date. Independently on numerical model analysis the measurements of real system can append the numerical methods. These experiments are oriented on the short-circuit current evaluation. The reactive current injection presented in [9] also can be treated as the injection or disturbance method. The method

based on reactive current injection allows to recognize steady state component of short circuit current. The phasor estimation is essential while steady state component of the short circuit current is evaluated [10, 11].

The analysis presented in the paper concerns on three-phase circuits. The grid parameters are recognized by injection of reactive current or short current impulse.

II. CONCLUSIONS

Assuming that the circuit model representing the power grid is linear the short-circuit current is equal to the sum of two components - steady state component and transient component. Steady state response is the sinusoidal function depending on voltage sources acting in the system. Each source has its share and this response does not depend on the time instant when short circuiting occurred. The steady state component can be computed using symbolic complex numbers method.

The starting value of short circuit current can be expressed as linear algebraic function of the capacitor voltages and inductor currents at the switching instant. The set of all capacitor voltages and inductor currents forms the system state. But for the chosen port only limited set of state variables influences on the port current while short circuit happens. Exists such port neighbourhood that only capacitors and inductors placed in this neighbourhood influence on the port current at the switching instant.

The rectangular current pulse is injected to port while the grid is examined. Recognized 2-port representing the part of circuit placed at the neighbour of the short circuited port is searched as one of two alternative circuits models: capacitive and inductive circuit. The parameters of these models can be elaborated from the measurements of the port voltage. As the result the short circuit current can be predicted from the data obtained while the experiment with pulse current injection is done.

Higher harmonics presence in experiments with LF MF exposure of biological samples

1st Roman Radil
*Dept. of Electromagnetic and
Biomedical Engineering
University of Zilina
Zilina, Slovakia
roman.radil@uniza.sk*

2nd Veronika Wohlmuthova
*Dept. of Electromagnetic and
Biomedical Engineering
University of Zilina
Zilina, Slovakia
veronika.wohlmuthova
@uniza.sk*

3rd Michal Labuda
*Dept. of Electromagnetic and
Biomedical Engineering
University of Zilina
Zilina, Slovakia
michal.labuda@uniza.sk*

4th Kristina Paulecova
*Dept. of Electromagnetic and
Biomedical Engineering
University of Zilina
Zilina, Slovakia
paulecova1@stud.uniza.sk*

Abstract—This paper deals with presence of higher harmonics within the driving signal of the exposure setup during experiments with microbiological samples, which could be potential source of discrepancies in the field of non-thermal low frequency magnetic field (LF MF) effects on biological samples.

The exposure setup comprises of two 1m long solenoid coils, which were developed to assure uniformity of applied LF MF in the exposed area within their cavity, where the biological samples are placed. To investigate non-thermal effects, the system was tested to produce magnetic fields up to 500 micro-Tesla at 50 Hz with almost no or negligible heating. The uniformity of LF MF was tested via numerical simulations and direct measurements of magnetic flux density using Narda analyzer NBM-550 with probe EPH-50D, under various conditions, e.g. outside the incubator, inside the incubator, with or without shielding plate, etc. Results of these techniques were comparable, which led to conclusion that the designed exposure setup is valid for testing with biological samples, and subsequently for full experimental work. However, the conducted experimental results remained inconsistent providing ambiguous and contradictory data regarding the biological reactions to applied LF MF.

During the search for the cause of these inconsistent results, studies from other research groups worldwide were reviewed. Based on these studies, establishment of correct and precise monitoring of magnetic field is a must for such type of experiments, as it is regarded as one of the initial steps towards unification of methodologies for assessment of biological effects of LF MF. Scientifically it is still a challenging task, especially when low-level (micro-Tesla range) magnetic fields at frequencies around 50 Hz are considered, because their generation, maintenance and control are usually aligned with the complex process of corresponding impedance matching. Moreover, this should be supported by background static, or geomagnetic field monitoring, because it was shown that the slightest differences in magnetic field parameters, such as frequency or flux density could lead to unpredictable inter- and/or intra- experimental errors.

Therefore, the focus of this article is on the optimized measurement procedures incorporating new sensor equipment, which are developed to better suit the requirements for monitoring physical quantities, specifically magnetic flux density, in the exposed area. In order to consider the actual levels of the magnetic field affecting the cell cultures during experiments, the differences between calculated and measured magnetic flux density values are evaluated. Measurements are performed, with regard to corresponding values of the electric current used to feed the

electromagnet during the experiments, using two specific sensors HMC5883L and MC858. Considering differences in specific sensor characteristics, the measurements are taken separately.

For the purpose of this article both measurements and analytical solutions are compared, however when evaluating individual experiments, the magnetic flux density values measured by the MC858 Sensor are considered more relevant than those measured via the magnetic compass HMC5883L. This is due to the advantages and limits of both sensors, where the HMC 5883L is designed primarily for static magnetic field measurements in three orthogonal axes, while the MC858 sensor is one-axis sensor but designed to measure time-varying magnetic field within the frequency range of 10–400 Hz. The calculation of magnetic field inside the solenoid is based on Biot-Savart law of an infinitely long solenoid, thus represents an ideal case, derived from the model. But previously performed numerical simulations have proven that uniformity of magnetic field inside the coils of finite length is maintained within the area of interest, despite the fact the intensity is different at the edges of both solenoids.

In general, the results show that the measured levels of magnetic flux density are lower than expected ones. For the driving signal of electric current $I_{AC} = 50$ mA, the measured magnetic flux density is 56.57% of the calculated; for $I_{AC} = 82.23$ mA, it is 60.29% of the calculated. More importantly, the analysis presented within this article reveals the presence of higher harmonic components, which influences the resulting magnetic field levels. The magnetic flux density within the central part of solenoid is formed by a superposition of individual harmonic components and a static component of the field. This could be one of the potential reasons for the discrepancy between the measured and theoretical magnetic induction values, as well as inconsistencies of performed biological experiments.

The source of these higher harmonic components will be subject to further investigation; however, for properly setting up the experimental conditions and verifying the selective effect of a specific frequency, it is clear that these harmonic components must be effectively filtered and driving signal should be adjusted accordingly. (*Abstract*)

Fabian Gil
 Military University of
 Technology
 Warsaw, Poland
 fabian.gil@wat.edu.pl

Stanislaw Osowski
 Warsaw University of
 Technology and Military
 University of Technology
 Warsaw, Poland
 stanislaw.osowski@pw.edu.pl

Abstract—This paper compares different solutions of the hybrid ensemble systems based on CNN networks in recognition of melanoma images. The CNN classifiers are used in two different roles. In the first, they serve as the source of numerical descriptors of the images. These descriptors after the selection procedure are applied as the input attributes to the classical support vector machine (SVM) classifiers combined in an ensemble. In the second approach, the ensemble is formed directly from the carefully selected CNN classifiers of different architectures. The performance of both approaches to the ensemble creation is checked in the task of recognition of images representing melanoma and non-melanoma lesions.

Keywords—ensemble of classifiers, melanoma recognition, CNN, feature selection.

I. INTRODUCTION

Classification problems of data belong to the classical task of artificial intelligence and machine learning. To achieve higher efficiency of the classification system the ensemble of classifiers composed of the independent units is usually built. The members of the ensemble should provide similar and possibly high efficiency in problem-solving. Aggregation of their results leads to better performance of the system.

II. HYBRID ENSEMBLE OF CLASSIFIERS

In general, the ensemble creation procedure consists of two main stages: 1) choosing and training the individual classifiers and 2) aggregating their results into a common decision of the ensemble (of potentially better accuracy, than its best unit). In this solution we will use the CNN classifiers. The CNN represents a multilayer structure, responsible for the generation of image numerical descriptors (performed in the locally connected layers). These descriptors are the basis for the creation of the input attributes to the final, fully connected classifier (usually softmax). This paper will investigate using different types of the final classifier, for example, support vector machine, combined with the additional stages of the feature selection. As a results the proposed hybrid system of the ensemble has the form, shown in Fig. 1.

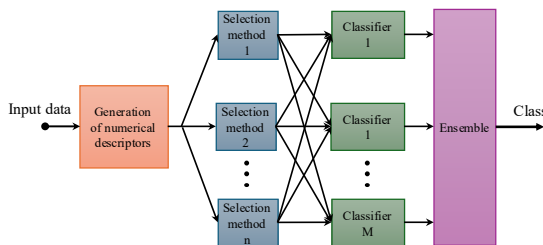


Fig. 1 The proposed general structure of the ensemble system.

Irrespective of the final classification stage applied in the system, the large population of image descriptors produced by the locally connected layers of CNN should be reduced to obtain better generalization ability of the system. In typical CNN classifiers applying softmax, the random selection is

usually applied by defining the proper dropout ratio (typically 50%). In the case of replacing softmax with a classical neural network (for example SVM), there is a need to reduce this number optimally. It is done by the application of some deterministic feature selection procedures. From many existing methods, we have chosen the following ones [1]: Fisher discriminant method (FD), Student T-test (T-test), Kolmogorov-Smirnov hypothesis (KS), Kruskal-Wallis test (KW), Correlation of input data with the class (CDC), Successive step-wise selection (SWF), Nearest neighbor analysis (NNA), and Relieff method (REL). The chosen methods define the descriptors according to the assumed mechanism of selection. These mechanisms differ a lot. Therefore, the final results of the application of the particular selection method are close to be independent.

III. THE DATABASE USED IN EXPERIMENTS

The numerical experiments comparing different approaches to ensemble creation have been performed using the melanoma database created at the National Institute of Oncology (NIO) in Warsaw [1]. It is a reasonably small database containing 134 images of melanoma and 112 images representing non-melanoma lesions. The images have been created using the dermoscope of the magnification 20x ad stored in JPEG format. The other database is the international set of data, called ISIC [1].

IV. RESULTS OF EXPERIMENTS

Transfer learning approach has been used in experiments. We have used 19 different architectures of CNN available in Matlab [2]. The have been subjected to fine tuning on the actual datase of melanoma. Their results have been aggregated by majority voting. All experiments have been repeated using 5-fold validation method. In all cases the ensemble, carefully selected, has produced better results than the best individual classifier. The confusion matrix of the ensemble for testing data in 5-fold cross validation is as follows.

$$C = \begin{bmatrix} 134 & 0 \\ 2 & 110 \end{bmatrix}$$

The melanoma has been recognized without any misclassification, while the best Resnet101 has committed 2 such misclassifications. In the case of ISIC database the differences between individual solution and the ensemble are much larger, as it is seen below. The best unit has not recognized 72 melanoma cases, while the ensemble only 50 (reduction of 22 errors).

Best individual	Ensemble
$C = \begin{bmatrix} 873 & 72 \\ 33 & 1510 \end{bmatrix}$	$C = \begin{bmatrix} 895 & 50 \\ 36 & 1507 \end{bmatrix}$

REFERENCES

- [1]. F. Gil F., “Zespoły sieci głębokich w rozpoznawaniu wybranych klas obrazów medycznych”, rozpr. dokt. WAT, 2024 (in Polish).
- [2]. Matlab user interface, MathWorks, Natick, USA, 2024.

Hybrid Order-Aware CNN–Vision-Language Model for LN-RADS–Based Lymph-Node Diagnosis

Grzegorz Gwardys
Faculty of Electronics and Information
Technology
Warsaw University of Technology
Warsaw, Poland
grzegorz.gwardys@pw.edu.pl

Maciej Jurewicz
Department of Artificial Intelligence,
Institute of Information Technology
Warsaw University of Life Sciences
Warsaw, Poland
maciej_jurewicz@sggw.edu.pl

Jarosław Kurek
Department of Artificial Intelligence,
Institute of Information Technology
Warsaw University of Life Sciences
Warsaw, Poland
jaroslaw_kurek@sggw.edu.pl

Cezary Chudobiński
Copernicus Regional Multi-Specialty
Oncology and Trauma Centre
Łódź, Poland
cezary.chudobinski@wp.pl

Bartosz Świdorski
Department of Artificial Intelligence,
Institute of Information Technology
Warsaw University of Life Sciences
Warsaw, Poland
bartosz_swidorski@sggw.edu.pl

Keywords: LN-RADS, Lymph-node ultrasound, Ordinal multi-task learning, Metastasis detection, Siamese network

I. INTRODUCTION

Lymph-node (LN) involvement is widely recognised as one of the strongest prognostic determinants in oncology—often surpassing primary-tumour size or histological subtype when selecting therapy and estimating survival [1]. The recently introduced LN-RADS (Lymph Node Reporting and Data System) [2] refines nodal evaluation from a binary “metastatic / benign” verdict to an ordinal six-point scale, offering a far richer depiction of disease burden. We investigate whether modern deep-learning pipelines can exploit this structured radiological knowledge more effectively than supervision that relies solely on histopathology.

II. METHODS

We build a three-branch hybrid model that fuses:

(i) a lightweight CNN (MobileNetV3-Small) to capture sonographic texture and shape cues; (ii) a frozen CLIP vision–language encoder used as a generic visual backbone, followed by a small MLP projection; (iii) a compact vector of LN-RADS–style radiological descriptors (e.g., cortical thickness, L/S ratio, hilum visibility).

The three embeddings are concatenated and fed to a shallow head that outputs a malignancy logit. Training minimizes binary cross-entropy for metastasis detection and, in parallel, an ordinal triplet loss applied to the fused embedding: samples with adjacent LN-RADS grades are pulled together, whereas distant grades are pushed apart. The LN-RADS labels thus shape the embedding space but are not predicted explicitly. We report uni-, bi- and tri-modal variants to assess the contribution of each modality.

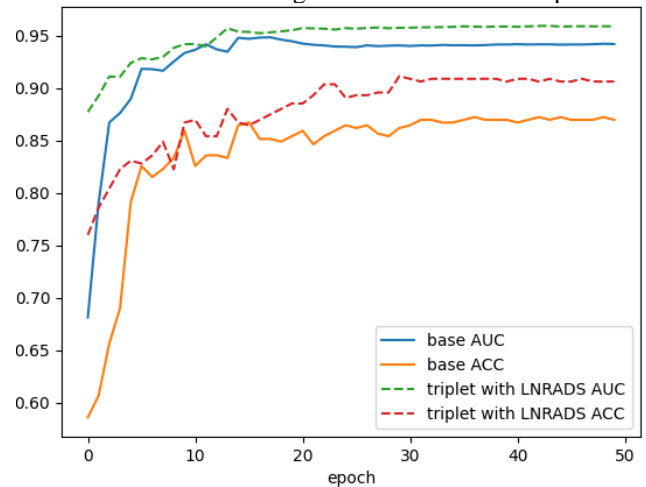
III. RESULTS

Experiments on an ultrasound dataset annotated both histopathologically and with LN-RADS grades reveal three key findings:

- Vision–language embeddings are strong standalone predictors. Using the frozen encoder as a feature extractor already produced $ACC \approx 0.79$ and $AUC \approx 0.85$ and accuracy ≈ 0.79 , underscoring the descriptive

strength inherent in language-aligned visual representations.

- Siamese multi-task training improves ordinal coherence. The tailored loss arranged inter-class distances to respect LN-RADS ordering, reduced ranking errors, and delivered predictions that align more closely with clinical expectations.
- The model leveraging all three branches together with the ordinal loss component achieves the highest performance ($ACC \approx 0.90$, $AUC \approx 0.95$). Below ACC and AUC values averaged over 5 folds across epochs.



IV. CONCLUSION

Integrating structured radiological expertise (LN-RADS), semantically enriched vision–language features, and order-aware metric learning yields a nuanced and interpretable diagnostic tool for LN assessment in ultrasound. The approach outperforms traditional binary pipelines, paving the way for more precise risk stratification and, ultimately, better-informed therapeutic decisions.

REFERENCES

- [1] A. T. Nguyen, M. Luu, V. P. Nguyen, *et al.*, “Quantitative nodal burden and mortality across solid cancers,” *J. Natl. Cancer Inst.*, vol. 114, no. 7, pp. 1003–1011, July 2022
- [2] C. Chudobiński, B. Świdorski, I. Antoniuk, and J. Kurek, “Enhancements in radiological detection of metastatic lymph nodes utilizing AI-assisted ultrasound imaging data and the lymph node reporting and data system scale,” *Cancers*, vol. 16, no. 8, Article 1564, Apr. 2024.

Impedance-Frequency Characteristics of Surface Dry EEG Electrodes Using an Agar-Based Phantom

Lubomir Trpis
Department of
Electromagnetic and
Biomedical Engineering
University of Zilina
Univerzitna 8215/1, 010 26
Zilina, Slovakia
trpis6@stud.uniza.sk

Maros Smondrk
Department of
Electromagnetic and
Biomedical Engineering
University of Zilina
Univerzitna 8215/1, 010 26
Zilina, Slovakia
maros.smondrc@uniza.sk

Veronika Wohlmuthova
Department of
Electromagnetic and
Biomedical Engineering
University of Zilina
Univerzitna 8215/1, 010 26
Zilina, Slovakia
wohlmuthova@stud.uniza.sk

Branko Babusiak
Department of
Electromagnetic and
Biomedical Engineering
University of Zilina
Univerzitna 8215/1, 010 26
Zilina, Slovakia
branko.babusiak@uniza.sk

This study focuses on the methodology for preparing and measuring the impedance-frequency characteristics of surface dry EEG electrodes manufactured by g.tec company. The electrode-skin interface is a well-known area and has been extensively studied in other studies. Human skin consists of several layers – epidermis, dermis, and hypodermis [1]. The outermost layer – the epidermis – serves as a protective barrier for subcutaneous tissue and internal organs. The uppermost sublayer of the epidermis – the stratum corneum – is a dry and oily tissue that represents the primary source of electrical resistance in surface biosignal acquisition [2]. Conductive gel is commonly used in practice to decrease the contact impedance between the electrode and the skin. However, conductive gels tend to dry out over time, significantly affecting the impedance at the electrode-skin interface. A modern alternative for surface biosignal acquisition is the use of dry electrodes, which form a thin moisture layer on the skin, partially replicating the function of conductive gel. Due to their specific shape and structural design, dry electrodes inherently provide lower impedance compared to Ag/AgCl electrodes used without conductive gel [3].

The impedance behavior of the electrode-skin interface can be modeled as a parallel combination of a resistor and a capacitor [4]. Based on this, a proper printed circuit board (PCB) developed in a previous study was used for measurements [5]. Three types of dry electrodes made of two different materials from g.tec company were measured. Two variants of Special Golden Alloy (SGA) electrodes were tested, differing in pin length – 7 mm and 16 mm. Additionally, a Special Conductive Polymer (SCP) electrode with a 7 mm pin length was measured. Electrical contact with the skin is basically achieved using eight thin electrode pins. For comparison purposes, a wet adhesive Ag/AgCl electrode containing conductive gel was also measured.

To ensure consistent measurement conditions, an agar-based phantom was used. The phantom was prepared using 300 ml of distilled water and 12 g of agar powder (corresponding to 4 g of agar powder per 100 ml of distilled water). After boiling and allowing the mixture to rest for approximately two minutes, the agar mixture was poured into a mold fabricated using 3D printing. Two adhesive electrodes (with the gel layer removed) were embedded into the surface layer of the phantom at a distance of 14 cm from each other. After that, the agar-based phantom was allowed to solidify in the fridge. Then, the measured electrode was placed at the center of the phantom, at the same distance – 7 cm – from both adhesive electrodes [5]. To ensure stable placement, custom 3D-printed housings were designed for each measured electrode. Each housing was constructed to support a 200 g weight. The weight was uniformly distributed to ensure consistent pressure and contact at the electrode-agar interface. The insertion depth of each electrode was limited to 1 mm to maintain surface measurement conditions, and to prevent damaging the phantom.

Measurements were conducted in a frequency range from 0.5 Hz to 1.1 kHz. The input signal was a sine wave with an amplitude of 5 V. The impedance of the measured electrode was calculated using

the mathematical equations described in the research by I. Kralikova, B. Babusiak, and M. Smondrk [5]. Each measurement session lasted approximately 75 minutes. The results provide valuable insights into the frequency response of dry electrodes and their behavior when in contact with the agar-based phantom. When comparing dry electrodes, the dry 7 mm SGA electrode demonstrated the best performance in terms of impedance magnitude. However, the smallest phase shift was observed with the dry 16 mm SGA electrode, indicating lower resistive-capacitive behavior. Nevertheless, the overall range of phase shift values among dry electrodes was above -50° in most frequencies, confirming their moderate resistive-capacitive behavior. Additionally, results for both dry SGA electrodes were in similar values and trends. The SCP electrode exhibited the highest impedance among the tested electrodes, but the phase shift remained consistently within the range from -50° to -40° . The data were also compared with results obtained from the wet adhesive Ag/AgCl electrode. In comparison, the wet adhesive Ag/AgCl electrode demonstrated the most stable results in both impedance magnitude and phase. This electrode also showed stable, yet moderate resistive-capacitive behavior in each measured frequency.

In conclusion, this methodology offers a reproducible and non-invasive approach for laboratory testing of the impedance characteristics of various types of surface electrodes.

Keywords—Artificial electrode-skin interface, Biosignal acquisition, Contact impedance, Dry EEG electrodes

REFERENCES

- [1] M. Maruccia and G. Giudice, “Basic Principles and New Perspectives Textbook of Plastic and Reconstructive Surgery.”
- [2] J. Heikenfeld *et al.*, “Wearable sensors: Modalities, challenges, and prospects,” Jan. 21, 2018, *Royal Society of Chemistry*. doi: 10.1039/c7lc00914c.
- [3] N. Faadhilah Afif, S. Harke Pratama, F. Haryanto, S. Nurul Khotimah, and Suprijadi, “Comparison of Wet and Dry EEG Electrodes Based on Brain Signals Characterization in Temporal and Anterior Frontal Areas Using Audio Stimulation,” in *Journal of Physics: Conference Series*, Institute of Physics Publishing, Jun. 2020. doi: 10.1088/1742-6596/1505/1/012069.
- [4] L. M. Ferrari, U. Ismailov, F. Greco, and E. Ismailova, “Capacitive Coupling of Conducting Polymer Tattoo Electrodes with the Skin,” *Adv Mater Interfaces*, vol. 8, no. 15, Aug. 2021, doi: 10.1002/admi.202100352.
- [5] I. Kralikova, B. Babusiak, and M. Smondrk, “Measurement of the conductive fabric contact impedance for bioelectrical signal acquisition purposes,” *Measurement (Lond)*, vol. 217, Aug. 2023, doi: 10.1016/j.measurement.2023.113005.

Influence of external electromagnetic field at mains frequency 50Hz on pacemakers

1st Michal Gala
*Dept. of Electromagnetic and
Biomedical Engineering
University of Zilina
Zilina, Slovakia*
michal.gala@uniza.sk
<https://orcid.org/0000-0002-4080-0729>

2nd Milan Smetana
*Dept. of Electromagnetic and
Biomedical Engineering
University of Zilina
Zilina, Slovakia*
milan.smetana@uniza.sk
<https://orcid.org/0000-0002-8419-5428>

3rd Ivana Galova
*Dept. of Electromagnetic and
Biomedical Engineering
University of Zilina
Zilina, Slovakia*
galova.ivka@gmail.com

4th Mariana Benova
*Dept. of Electromagnetic and
Biomedical Engineering
University of Zilina
Zilina, Slovakia*
mariana.benova@uniza.sk
<https://orcid.org/0000-0002-5324-4637>

Abstract— The expansion of modern information and communication technologies has led to an increasing presence of electromagnetic field (EMF) sources in the environment, raising concerns about electromagnetic interference (EMI), particularly with implantable electronic devices, such as pacemakers. These devices rely on the accurate sensing and modulation of the heart's electrical activity. Exposure to external EMF can lead to the induction of electrical voltages on the pacemaker electrodes, which can be misinterpreted as a physiological signal. Such misinterpretation can result in erroneous therapy, such as temporary suppression of stimulation or switching to asynchronous mode, which can lead to the development of arrhythmias or other clinically significant conditions. Although these phenomena are mostly transient and disappear after leaving the interference source zone, patients entirely dependent on the correct function of the pacemaker represent a risk group. The present study, with its significant findings, aims to evaluate the impact of an electromagnetic field (EMF) with a frequency of 50 Hz on the functionality of the pacemaker. Specifically, it investigates the occurrence of voltage induced on electrodes due to external EMF, while two types of overhead power lines were chosen as sources: 2x 110 kV and 1x 400 kV. The work employed numerical simulations and real measurements to determine the values of electric field intensity and magnetic field induction, utilizing numerical methods (FEM) and analytical calculations. The induced voltages were evaluated separately for unipolar and bipolar electrode arrangements due to differences in the effective induction area. The results show that the unipolar electrode arrangement is significantly more susceptible to the occurrence of induced voltage due to the larger area of the induction loop,

especially under adverse conditions such as low conductor height above the ground and high current in the line. In the most unfavourable case, the effective induced voltage reached values of up to 336.73 μV for unipolar and 37.08 μV for bipolar configurations. These findings, along with the study's comprehensive approach, underscore the importance of considering both elements of the electromagnetic field in simulation models. The accuracy of the numerical simulations was verified using measurements in a real environment with deviations ranging from 2% to 15%. The deviations were affected by the tolerance of the measuring instruments, surrounding objects (e.g., cars, wet soil), and simplifications in the models. In vitro testing with four different types of pacemakers from various manufacturers revealed varying immunity to EMI. Some devices adjusted the sensitivity threshold correctly, while others responded incorrectly by switching to asynchronous mode or completely blocking stimulation. These differences indicate varying degrees of robustness among devices, depending on the manufacturer, despite similar programming. The results underscore the importance of a comprehensive assessment of electromagnetic compatibility (EMC) in the design of medical devices, as well as the implementation of effective preventive measures. It is essential to ensure the standardization of EMI protection mechanisms, increase awareness among medical personnel and patients, and update standards regarding EMF exposure, especially in areas with increased loads, such as industrial zones or areas near high-voltage power lines. Although the values of the induced voltages are relatively low, their impact on pacemaker operation may be clinically relevant, especially in patients with unipolar electrode arrangements.

Interactive Visualization of Data from a Ceramic Printer

Lenka Šroubová

Department of Electrical and
Computational Engineering
University of West Bohemia in Pilsen
Pilsen, Czech Republic
lsroubov@fel.zcu.cz

Karel Slobodník

Department of Electrical and
Computational Engineering
University of West Bohemia in Pilsen
Pilsen, Czech Republic
karels1@fel.zcu.cz

Petr Kropik

Department of Electrical and
Computational Engineering
University of West Bohemia in Pilsen
Pilsen, Czech Republic
pkropik@fel.zcu.cz

Jakub Racek

Department of Electrical and
Computational Engineering
University of West Bohemia in Pilsen
Pilsen, Czech Republic
racekj@students.zcu.cz

Michal Prokeš

Department of Electrical and
Computational Engineering
University of West Bohemia in Pilsen
Pilsen, Czech Republic
prokes@students.zcu.cz

Jan Rejzek

Department of Electrical and
Computational Engineering
University of West Bohemia in Pilsen
Pilsen, Czech Republic
rejzek17@students.zcu.cz

Abstract—This project aims to develop a system for interactive visualization of data from the KEPrint ceramic 3D printer using augmented reality and mixed reality (AR/XR) technologies. The printer will be equipped with sensors monitoring key operational parameters such as temperature, pressure, axis movement, and printing status. These sensor data will be transmitted to an MQTT broker, and then delivered to subscribers represented by end-user devices, including smartphones, tablets, AR/XR headsets, and servers (web servers, database servers). Users will be able to remotely view the current status of the printer, even if it is located in a restricted laboratory environment. This approach enables safe and informed access to laboratory equipment that may be inaccessible due to safety regulations, GDPR constraints, or health-related limitations.

Keywords—3D printing, 3D ceramic printer, augmented reality, mixed reality, sensor data acquisition, communication, real-time data visualization.

I. INTRODUCTION

A prototype of the 3D ceramic printer KEPrint has been developed at the University of West Bohemia [1], [2], [3]. Previously, workers had to visit the lab to monitor parameters personally. The printer now has sensors, allowing staff to monitor data remotely on a graphical web-based user interface and on an augmented reality device.

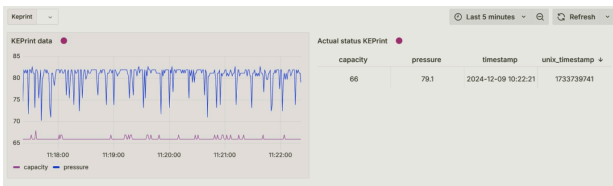


Fig. 1. Data Interactive Visualization from a Ceramic 3D printer

II. DATA INTERACTIVE VISUALIZATION

Sensor data from the KEPrint ceramic 3D printer was successfully integrated into an AR/XR-based visualization system. Pressure and reservoir capacity were measured using a water pressure sensor and an ultrasonic distance sensor, respectively, with data processed by an ESP32 microcontroller. The values were displayed locally on an I2C LCD and transmitted via MQTT in JSON format to a broker, enabling scalable integration of additional devices. The data were stored in an InfluxDB database and

visualized through web pages using dynamic graphs and tables in real time (Fig. 1). Furthermore, the system was extended to Microsoft HoloLens 2 using our in-house application implemented in Unity. This implementation enables remote, interactive laboratory equipment monitoring through mixed reality (Fig. 2), enhancing accessibility and safety.



Fig. 2. Monitoring of equipment through mixed reality

III. CONCLUSION

Sensor data from the KEPrint printer is processed and visualized in real time via MQTT, InfluxDB, and Grafana, with AR display enabled through HoloLens 2 and other mobile devices. This approach facilitates safe and informed access to laboratory equipment while concomitantly limiting unnecessary movement of people in the laboratory. This approach is now gradually being extended to other laboratory equipment.

ACKNOWLEDGMENT

This research has been supported by the University of West Bohemia and the University Students Project SGS-2024-025.

REFERENCES

- [1] SLOBODNÍK, K.; ŠROUBOVÁ, L.; SPURNÝ, R.; ŠEBELE, J. Design and Control of Ceramic 3D Printer. In: Proceedings of 2024 ELEKTRO (ELEKTRO), Zakopane, Poland. Piscataway: IEEE, 2024. ISBN 979-8-3503-7235-9.
- [2] SLOBODNÍK, K.; ŠROUBOVÁ, L.; SPURNÝ, R.; HEIMRATH, M. Extruder Design for 3D Printing of Ceramic Materials. In: Proceedings of 2023 24th International Conference Computational Problems of Electrical Engineering (CPEE 2023). Piscataway: IEEE, 2023. ISBN 979-8-3503-3034-2.
- [3] SLOBODNÍK, K.; PROKEŠ, M.; REJZEK, J.; ŠROUBOVÁ, L. Numerical simulation of ceramic material extrusion. In: 2024 25th International Conference on Computational Problems of Electrical Engineering (CPEE). Piscataway: IEEE, 2024. ISBN 979-8-3315-0664-3.

Limits of Large Language Models in Map Navigation and Spatial Reasoning

Tomasz Les
Faculty of Electrical Engineering
Warsaw University of Technology
Warsaw, Poland
tomasz.les@pw.edu.pl

Bartosz Sawicki
Faculty of Electrical Engineering
Warsaw University of Technology
Warsaw, Poland
bartosz.sawicki@pw.edu.pl

Abstract—Large Language Models (LLM) often fail to navigate text-based labyrinths and pixelated maps, struggling with simple spatial tasks and landmark interpretation. These issues highlight gaps in reasoning and planning. Our experiments will assess these limitations using controlled tasks to analyse model behaviour and recurring error patterns. Several methods to improve correctness of LLM responses have been presented.

Index Terms—LLM, navigation

I. INTRODUCTION

Advances in map comprehension and navigation by LLM open transformative possibilities in domains such as autonomous robotics, assistive technologies, and geo-information systems. For example, LLMs that interpret textual or visual maps could guide delivery robots through dynamically changing environments, assist visually impaired users in indoor navigation, or enable conversational interfaces to perform spatial queries and generate route maps interactively [1], [2].

Understanding and navigating map-like environments, whether conveyed through text or pixelated images, poses a substantial challenge to current large-language models (LLMs). We explore these capabilities in two complementary domains: (i) *text-based labyrinths*, as exemplified by the MANGO benchmark that encompasses 53 text adventure mazes and hundreds of navigation queries formulated from sparse walk-throughs [3]; and (ii) *pixel-map outdoor navigation*, as addressed by MapBench, which offers more than 1,600 pathfinding tasks in 100 diverse real-world map images [4].

In the textmaze domain, models are asked to infer both route planning (“How to reach the Attic from west of House?”) and positional reasoning (“If you go north then east from Cellar, where are you?”) based on limited textual guidance. Although intuitively straightforward to humans, even state-of-the-art LLMs such as GPT4 perform poorly in these tasks [3].

In the pixel-map domain, models are presented with static, landmark-annotated images and tasked to autonomously generate natural language instructions for traversing from a start to a goal location. MapBench demonstrates that prominent vision language models struggle significantly in spatial reasoning and structured decision making, both under zero-shot prompting and Chain-of-Thought frameworks [4].

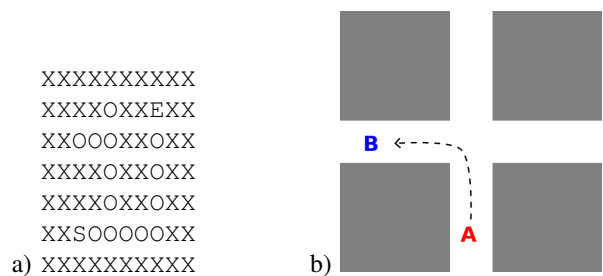


Fig. 1. Examples of maps used in experiments: a) text based labyrinth, b) graphic file of crossroad.

II. EXPERIMENTS

Our evaluation setup is based on two types of maps (as presented in Fig. 1) with various prompting techniques. The analysis reveals common problems in maintaining a clear internal understanding across different types of input. Each input type has its own issues: text makes it hard for models to build structured memory, while images make it harder to connect perception with spatial reasoning.

The experiments showed that the most advanced current models (like OpenAI gpt-5) with reasoning mode could successfully perform navigation tasks. However, similar accuracy with much smaller computational cost could be achieved using simpler models with careful design of prompting strategy and data preparation.

REFERENCES

- [1] J. Lin, H. Gao, X. Feng, R. Xu, C. Wang, M. Zhang, L. Guo, and S. Xu, “Advances in embodied navigation using large language models: A survey,” *arXiv preprint arXiv:2311.00530*, 2023, survey of LLMs in embodied navigation tasks.
- [2] S. Song, S. Kodagoda, A. Gunatilake, M. G. Carmichael, K. Thiyagarajan, and J. Martin, “Guide-llm: An embodied llm agent and text-based topological map for robotic guidance of people with visual impairments,” in *arXiv preprint arXiv:2410.20612*, 2024, textual-map guided navigation for assistive technology.
- [3] P. Ding, J. Fang, P. Li, K. Wang, X. Zhou, M. Yu, J. Li, M. R. Walter, and H. Mei, “Mango: A benchmark for evaluating mapping and navigation abilities of large language models,” 2024, text-adventure maze navigation benchmark.
- [4] S. Xing, Z. Sun, S. Xie, K. Chen, Y. Huang, Y. Wang, J. Li, D. Song, and Z. Tu, “Can large vision language models read maps like a human?” *arXiv preprint arXiv:2503.14607*, 2025, mapBench: pixelated map navigation benchmark.

Low-Cost Randomness Extraction from Power Line Voltage Signal

Piotr Witkowski
Faculty of Electrical Engineering
Warsaw University of Technology
Warsaw, Poland
piotr.witkowski@pw.edu.pl

Bartosz Sawicki
Faculty of Electrical Engineering
Warsaw University of Technology
Warsaw, Poland
bartosz.sawicki@pw.edu.pl

Abstract—This study investigates a methods to convert analog voltage signals into binary random sequences by analyzing their period durations and statistical patterns. It includes the development of efficient methods for extracting random sequences from the natural noise present in power grid signals.

Index Terms—randomness, entropy

I. INTRODUCTION

In this study, we investigate a method for transforming an analog voltage signal into a binary sequence by examining its periodicity and statistical properties. Leveraging the physical characteristics of analog signals to generate binary sequences presents an attractive alternative to traditional entropy sources—especially in the context of low-cost, hardware-based random number generator (RNG) solutions. Previous work has demonstrated that architectures with dual entropy cores based on chaotic maps (e.g., Bernoulli map) successfully produce high-quality randomness [1]. Similarly, deterministic chaos extracted from analog circuits such as phase-locked loops (PLLs) has been shown to approximate white noise and serve as a high-entropy bit source [2]. Our approach centers on comparing successive signal periods—a simple method aligned with established entropy extraction techniques—and assessing the resulting binary sequences through entropy and compressibility metrics [3].

The methodology begins with extracting a vector of full and half-period durations from a continuous voltage signal. Two approaches are applied: zero-crossing detection and identification of signal extrema (local maxima and minima). For both methods, histograms of the obtained period durations are constructed to assess the underlying statistical distributions. Preliminary assumptions suggest the possibility of normal distributions, which are verified using visual analysis and descriptive statistics.

Following period extraction, a binary transformation is applied: each period is compared to the previous one, and assigned a value of 1 if it is longer, or 0 if it is shorter. The resulting binary sequence is then subjected to basic randomness quality assessments. These include entropy calculation and evaluation of compressibility using standard data compression techniques, aiming to approximate the unpredictability of the generated sequence.

To further examine the robustness of this signal-based binary generation, low-pass filters are applied to the original analog signal. The impact of filtering on the randomness of the binary output is measured and compared. As anticipated, the application of low-pass filters reduces high-frequency content and thereby lowers the entropy of the resulting sequence, demonstrating the sensitivity of the method to signal smoothing.

This approach opens up potential applications in low-cost, hardware-based entropy sources and randomness evaluation in analog-to-digital signal transitions.

REFERENCES

- [1] I. G. Cicek, A. E. Pusane, and G. Dundar, “A new dual entropy core true random number generator,” *Analog Integrated Circuits and Signal Processing*, vol. 81, no. 1, pp. 61–70, 2014, prototype passed NIST 800-22 tests and uses Bernoulli map entropy cores.
- [2] K. Demir and S. Ergun, “An analysis of deterministic chaos as an entropy source for random number generators,” *Entropy*, vol. 20, no. 12, p. 957, 2018, compares bounded/unbounded chaos from PLL devices with Gaussian white noise.
- [3] H. Zhou and J. Bruck, “Linear extractors for extracting randomness from noisy sources,” in *2011 IEEE International Symposium on Information Theory Proceedings*. IEEE, 2011, pp. 1738–1742.

Machine learning In Industrial Cyberthreat Detection*

1st Mateusz Praniuk

Poznan University of Technology
Poznań, POLAND
praniukmateusz@gmail.com

2nd Maksymilian Roj

Poznan University of Technology
Poznań, POLAND
maks@rscom.pl

3rd Janusz Pochmara

Poznan University of Technology
Institute of Automatic Control and Robotics
Poznań, POLAND
janusz.pochmara@put.poznan.pl

4th Krzysztof Kolanowski

Poznan University of Technology
Institute of Automatic Control and Robotics
Poznań, POLAND
krzysztof.kolanowski@put.poznan.pl

5th Aleksandra Świetlicka

Poznan University of Technology
Institute of Automatic Control and Robotics
Poznań, POLAND
aleksandra.swietlicka@put.poznan.pl

In the era of Industry 4.0, industrial networks are increasingly exposed to cyber threats, especially those targeting programmable logic controllers (PLCs). As infrastructure becomes more interconnected and digitized, the risk of cyber-attacks increases significantly, potentially resulting in severe consequences for operational safety and continuity [1].

This project presents a Python-based anomaly detection system aimed at improving cybersecurity in such environments. It performs real-time analysis of PLC memory and network traffic to identify unauthorized activity, such as malicious Modbus TCP or S7COMM packets and irregular data behavior, without relying on predefined attack signatures.

The urgency for better protection is underscored by high-profile incidents like the Stuxnet worm [2] and the Colonial Pipeline ransomware attack [3], both of which exposed serious vulnerabilities in industrial systems. These cases demonstrate the need for continuous monitoring and proactive detection mechanisms.

To address these challenges, the proposed system employs machine learning—specifically One-Class Support Vector Machines (SVMs)—to learn the normal operational patterns of an industrial process and detect deviations that may signal threats. SVMs are ideal for this application due to their effectiveness in distinguishing outliers within high-dimensional data [4].

A fully virtualized testbed was developed to simulate real-world attack scenarios, allowing the system to reliably differentiate between legitimate operations and malicious actions. Python was chosen for attack simulation because of its flexibility and robust libraries for communicating with PLCs. The system emphasizes network traffic analysis, which helps to detect suspicious communication behaviors and protocol misuse.

By analyzing both the PLC's internal memory state and external traffic in real time, the system identifies threats like unauthorized register modifications and abnormal data flows. This dual approach enhances detection accuracy without adding significant computational overhead.

Implemented in a virtual environment using Kali Linux machines, the system achieved promising results, with a detection accuracy of 94

The solution is modular, lightweight, and adaptable, making it suitable for a variety of industrial environments. It demonstrates the effectiveness of unsupervised machine learning techniques in protecting critical infrastructure, particularly in situations where conventional IT security tools are insufficient to address domain-specific threats [5].

In conclusion, this project shows how artificial intelligence can be practically integrated into industrial cybersecurity strategies, providing visibility, resilience, and adaptability against evolving threats. Continued development and implementation of such solutions are essential for ensuring the security and autonomy of modern industrial systems.

REFERENCES

- [1] S. Morgan, "Cyberwarfare 2021 Report," Jan. 2021, accessed: 2025-05-29. [Online]. Available: <https://cybersecurityventures.com/wp-content/uploads/2021/01/Cyberwarfare-2021-Report.pdf>
- [2] T. M. Chen and S. Abu-Nimeh, "Lessons from stuxnet," *Computer*, vol. 44, no. 4, pp. 91–93, 2011.
- [3] J. Beerman, D. Berent, Z. Falter, and S. Bhunia, "A review of colonial pipeline ransomware attack," in *2023 IEEE/ACM 23rd International Symposium on Cluster, Cloud and Internet Computing Workshops (CCGridW)*, 2023, pp. 8–15.
- [4] J. Cervantes, F. Garcia-Lamont, L. Rodríguez-Mazahua, and A. Lopez, "A comprehensive survey on support vector machine classification: Applications, challenges and trends," *Neurocomputing*, vol. 408, pp. 189–215, 2020.
- [5] L. Xuan and L. Yongzhong, "Research and implementation of modbus tcp security enhancement protocol," *Journal of Physics: Conference Series*, vol. 1213, no. 5, p. 052058, jun 2019.

Mathematical Model of a Saturated Synchronous Motor in Orthogonal d-q Axes as an Element of a Microgrid

Oksana Hoholyuk
Institute of Power Engineering and Control Systems
Lviv Polytechnic National University
Lviv, Ukraine
oksana.p.hoholyuk@lpnu.ua

Petro Gogolyuk
Institute of Power Engineering and Control Systems
Lviv Polytechnic National University
Lviv, Ukraine
petro.f.hoholiuk@lpnu.ua

A mathematical model of a saturated synchronous motor in orthogonal d-q axes has been created for the analysis of electromagnetic and electromechanical transients and steady-state conditions, taking into account the nonlinearity of the Weber-ampere characteristic of the main magnetic circuit of its magnetic core and the mutual cross-magnetic coupling between the d-q axes and the active power loss in it. The model is formed in the normal Cauchy form and can be easily adapted for use in computer mathematics software environments. The model provides the ability to take into account the mutual influence of the circuit, mode and parametric features of the synchronous motor and the elements of the microgrid in the physical phase a, b, c coordinates.

Key words – synchronous motor, mathematical model, microgrid.

I. INTRODUCTION

An important area in the development of intelligent power supply systems (PSSs), or microgrids, involves optimizing their operating modes and processes in the presence of synchronous motors (SMs) [1–4]. A key challenge in the study of such systems is the analysis of electromagnetic and electromechanical transient processes that occur during asynchronous starts and self-starts of SMs, as well as during steady-state periodic operations.

A modern and effective approach to studying these processes is mathematical modeling using advanced software platforms and computer-based mathematical tools. The investigation of transient phenomena in branched PSSs supplying dynamic loads, with synchronous motors present, becomes a complex scientific and engineering problem—particularly when considering schematic configurations, operating conditions, and parametric factors, including the nonlinear characteristics of the electrical and magnetic circuit components.

Previous works [1–4] have examined the influence of auxiliary winding configurations and capacitor capacitance on the parameters of steady-state operation and starting characteristics of a compensated induction motor (IM). However, these studies do not address the role of the motor as an integrated element of the power supply system. The purpose of this work is to address the problem of mathematical modeling of a saturated synchronous motor as a functional component of an electrical or power supply system.

II. FORMATION OF MATHEMATICAL MODEL

The mathematical model of a saturated synchronous motor is developed in rotor-oriented, moving orthogonal d–

q coordinate frames for voltages, currents, flux linkages, and magnetomotive forces, with consideration of active power losses in the magnetic core steel.

Model validation was carried out using an asynchronous machine with real physical parameters. The magnetic circuit's Weber–Ampere characteristic was approximated by a polynomial, from which the static magnetic reluctance characteristic was derived. The simulation yielded time-domain curves of key parameters during direct start-up of the induction motor (IM), including the phase voltage of the IM, the voltage across the compensating capacitor, the motor's input current, and the flux linkage referred to the main winding from the fundamental magnetic flux, among others.

CONCLUSION

A mathematical model of a saturated synchronous motor in orthogonal d-q coordinates has been created for the analysis of transients and steady states as an element of an electrical or electrical power distribution system, taking into account the stator winding connection schemes and the parameters of its electrical circuits, the nonlinearity of the magnetization characteristic of the main magnetic circuit of the magnetic core, the cross-magnetic coupling between orthogonal axes and the active power losses in it. The mathematical model is formed in the normal Cauchy form, which allows expanding its capabilities during the study of transients and steady states in complex electrical and power supply systems to solve specific problems of analysis and synthesis of such systems.

REFERENCES

- [1] D. C. Aliprantis, S. D. Sudhoff and B. T. Kuhn, "A synchronous machine model with saturation and arbitrary rotor network representation," *IEEE Transactions on Energy Conversion*, 2025, Vol. 20, No.3, pp.584-594, DOI: <https://doi.org/10.1109/TEC.2005.845455>.
- [2] B. Singh, A. K. Chandel, and A. Kumar, "Analysis of Saturated Synchronous Machine considering d-q Axis Coupling Reactance," *Proceedings of the Second International Conference on Research in Intelligent and Computing in Engineering, ACSIS*, 2017, Vol. 10, pp. 329–334, DOI:<http://dx.doi.org/10.15439/2017R60>.
- [3] J. Tamura, and I. Takeda, "A new model of saturated synchronous machines for power system transient stability simulations," *IEEE Transactions on Energy Conversion*, 1995, Vol. 10, No. 2, pp. 218–224, DOI: <https://doi.org/10.1109/60.391885>.
- [4] A. M. El-Serafi, and A. S. Abdallah, "Saturated synchronous reactances of synchronous machines," *IEEE Transactions on Energy Conversion*, 1992, Vol.7, No.3, pp.570-579.

Measurement of variation characteristics on electric field peak value due to microgap ESD

Ken Kawamata
 Department of Electrical and
 Electronic Engineering
 Tohoku Gakuin University
 Sendai, Miyagi, Japan
 kawamata@mail.tohoku-gakuin.ac.jp

Shinobu Ishigami
 Department of Electrical and
 Electronic Engineering
 Tohoku Gakuin University
 Sendai, Miyagi, Japan
 shinobu@mail.tohoku-gakuin.ac.jp

Osamu Fujiwara
 Emeritus professor
 Nagoya Institute of Technology
 Nagoya, Aichi, Japan
 o.fujiwara@nitech.jp

Abstract—The peak value of the transient electric field generated by micro-gap ESD with a voltage below 1 kV, which is feared to be an EMI source, was investigated experimentally. The measurements were performed using a pair of spherical electrodes as a reference model of discharge and a FLHA suitable for wideband time domain measurements. As a result, the transient electric field showed a peak at a discharge voltage of about 600 V. It was also confirmed that the roughness of the electrode surface affects the variation in the radiation field.

Keywords—ESD, transient electric field, EMI, a pair of spherical electrodes, FLHA, surface roughness

I. INTRODUCTION

The transient EM (electromagnetic) field caused by ESD (electrostatic discharge) has a serious impact on the operation of high-performance digital electronic devices and IT devices. In particular, the EM noise caused by micro-gap ESD with a voltage below 1 kV becomes a steep and extremely broadband impulsive EM noise source. However, the characteristics of EMI caused by ESD have not been fully elucidated, making it difficult to computation models and implement fundamental EMC countermeasures. Therefore, the electric field peak value was examined to clarify the relationship between the discharge parameters and the radiated transient electric field.

II. EXPERIMENTAL SETUP AND RESULTS

The measurement setup [1] was shown in Fig.1. The system consists of a pair of spherical electrodes made by brass boll, a high voltage D.C. power supply (0-1 kV), high resistance lines and a lumped resistance (30 kΩ, 1 MΩ), a folded long hexagon antenna (FLHA, 500 MHz - 20 GHz) shown in Fig. 2, and a digital oscilloscope (20 GHz, 50 GS/s). The distance between the electrode and the FLHA is 1 m, and the diameter of electrodes is 30 mm. The experimental parameters are the discharge voltage and the electrode surface roughness. The electrode surface was finished with roughness of 1 μm and 12 μm. Voltages were applied from 400V to 800V in 50V increments. In the experiment, with a specified voltage applied, the electrodes were moved closer at a speed of 5.0 mm/s, and the received EM field waveform when a discharge occurred was measured with the oscilloscope.

Fig. 3 shows an example waveform of the received electric field caused by ESD. The field peak value was measured by a peak to peak value of the waveform. Fig. 4 shows a relationship between discharge voltage and electric field strength, electrode roughness is 1 μm. The results are marking 100 results of 400 experiments. The red diamond marks are indicated the average value of the 400 experiments. The field peak values were proportion to the discharge voltage in voltage range from 400V to 600V. The electric field strength reached its peak at a discharge voltage of 650 V. And then, 650V or more, the electric field strength varied widely and the

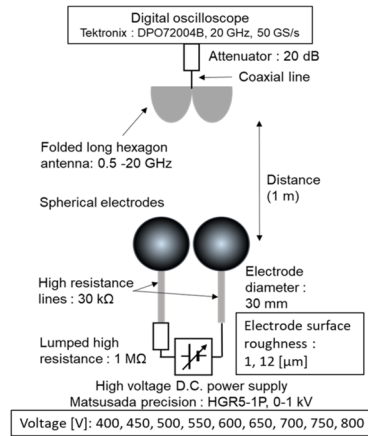
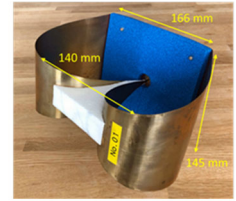
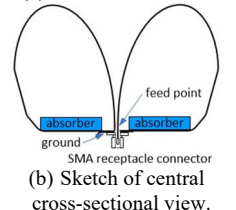


Fig. 1 Experimental setup.



(a) Photo of the FLHA.



(b) Sketch of central cross-sectional view.

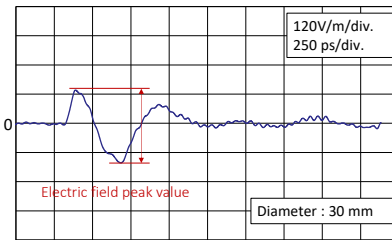


Fig.3 Example waveform of the received electric field waveform.

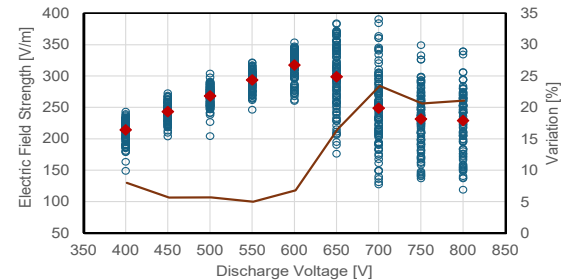


Fig.4 Relationship between discharge voltage and electric field peak value and its variation in the 1 μm electrode roughness.

average values were decreased. In voltage below 600 V, the variation characteristic is small at 6.3% or less, and no effect of electrode surface roughness was observed. On the other hand, at 650 V or more, the variation was increased to 20%.

III. CONCLUSION

The variation of electric field strength was relatively stable in below 600 V, and no effect of the electrode surface roughness was observed. On the other hand, the variation was large for smooth electrodes in discharge voltage over 650 V.

REFERENCES

[1] K. Kawamata, et al., Proc. of Int'l Symposium on 2024 EMC Europe, OS-ESD, 2024 Sept., Belgium.

Methodology for assesment of induced voltage on human body in the vicinity of overhead electric lines

1st Roman Radil
Dept. of Electromagnetic and
Biomedical Engineering
University of Zilina
Zilina, Slovakia
roman.radil@uniza.sk
<https://orcid.org/0000-0002-7883-6065>

2nd Ladislav Janousek
Dept. of Electromagnetic and
Biomedical Engineering
University of Zilina
Zilina, Slovakia
ladislav.janousek@uniza.sk
<https://orcid.org/0000-0002-4823-8910>

3rd Milan Smetana
Dept. of Electromagnetic and
Biomedical Engineering
University of Zilina
Zilina, Slovakia
milan.smetana@uniza.sk
<https://orcid.org/0000-0002-8419-5428>

4th Maroš Šmondrk
Dept. of Electromagnetic and
Biomedical Engineering
University of Zilina
Zilina, Slovakia
maros.smondrk@uniza.sk
<https://orcid.org/0000-0001-8216-3214>

Abstract— The article focuses on non-thermal biological effects of the grid frequency electromagnetic field (EMF) generated in vicinity of high voltage electric overhead lines. More exactly, it deals with the assessment of voltages or charges induced on a surface of human's body in the area near extra high voltage overhead power lines. This problematic is a part of a methodology for assessment of the intersections of cycling communications with high voltage electric overhead lines. Cyclists crossing high voltage electric overhead lines usually undergo the risk of electroshock, which might lead to the loss of concentration or acute paralysis and secondary serious injuries.

While the specific (thermal) biological effects of EMF are regulated through the guidelines of the International Commission on Non-Ionizing Radiation Protection and reflected in national regulations, the non-specific (non-thermal) ones are still not sufficiently addressed despite the emerging scientific evidence. The reason is, that this scientific area, especially within the low frequency range (1 - 300 Hz) is characteristic by contradictory results, methodological ambiguities and gaps of knowledge. Probably the most challenging research tasks incorporate description of general physical mechanism of the EMF action at molecular level, unification of methodology for assessment of biological effects of such field levels, as well as assessment and specification of long-term effects related with occupational exposure.

However, even within the area of short-term effects, there are scientifically valuable and unsolved problems, that are worth targeting. The known short-term effects of grid frequency EMF are connected to reversible changes on excitable cells, electric charge effects at the skin surface, heart rate variation or a stimulation of nerves and muscles experienced as a tingling

sensation. To this date, within Slovakia region there are multiple reports from cyclists, who experienced unpredictable sensation of electric discharge while crossing under the high or extra high voltage electric overhead lines. Lots of these reports are sent from the locality of Varin near Zilina, where there is probably one of the most frequent and exposed crossings of cycling routes and extra high voltage electric overhead lines in Slovakia. Since, there is no regulatory standard, or guideline for the assessment of the intersections of cycling communications with high voltage electric overhead lines in Slovakia, development of such a methodology is of the utmost importance.

Crucial part of this methodology is represented by description of the mechanism of electric charge transmission and distribution on the body surface. This description could be derived based on the electromagnetic induction phenomena. Thus, in the case of this study, the voltage changes within the specific positions on body surface are measured using electrostatic voltmeter. Moreover, the portable oscilloscope with high voltage probes is used to monitor the voltage levels at different locations in the vicinity of extra high voltage electric overhead lines, starting directly under the transmission lines.

These measurements are preliminary and are meant to test and optimise a designed methodology. The measured data are evaluated and presented to depict a preliminary picture regarding the exact levels of electric voltages, and potential gradients, which should indicate the distribution of electric charges on human's body surface.

Knowledge base gained through these research activities is the key stone to setup applicable and effective measures for minimization of associated health risks. (*Abstract*)

Modeling of the Electric Field Generated in the Human Body by Endovascular Electrodes

Jacek Starzyński

Warsaw University of Technology, Poland

This study presents the development of an individualized, anatomically realistic model of a section of the human body, incorporating thin-walled, delicate electrodes in the form of endovascular stents. The purpose of this model is to enable accurate simulation of the electric field generated within biological tissues by the application of phase-shifted radio-frequency voltages between multiple such electrodes. This excitation is intended to produce a rotating electric field of relatively high amplitude (200–400 V/m) within a targeted region of the body.

The primary research objective is to determine the extreme values of the electric field intensity and current density in the immediate vicinity of the stent electrode. These electrodes are typically composed of fine wire or a mesh structure with narrow bridging elements. Such a configuration may cause localized field amplification near the electrode surface, which is undesirable from a medical standpoint due to potential tissue damage or overstimulation.

Accurate modeling of the endovascular stent electrode poses a significant challenge owing to the substantial disparity in scale between the resolution of MRI data—used to construct the anatomical model—and the minute dimensions of the electrode's wire or mesh bridges. This paper describes the numerical and geometric techniques employed to achieve a high-fidelity representation of the electrode geometry while maintaining reasonable computational complexity.

Modelling of Chaotic Phenomena in an Electric Arc Furnace System

Piotr Witkowski

Institute of Theory of Electrical Engineering, Measurement and Information Systems, Warsaw University of Technology
Warsaw, Poland

Radosław Roszczyk

Institute of Theory of Electrical Engineering, Measurement and Information Systems, Warsaw University of Technology
Warsaw, Poland

Abstract—The paper presents a mathematical model of complex nonlinear phenomena occurring in an AC electric arc furnace system, which exhibits chaotic dynamics in the initial stages of steel smelting. The use of the hybrid Cassie–Mayr model and the Chua's circuit allowed modelling changes in the electric arc conductance, which are the result of unpredictable changes in the arc length due to the behaviour of plasma in a chaotic electromagnetic field. The dynamics of the electrical characteristics of arcs contribute to the generation of a wide spectrum of electromagnetic interferences that cause asymmetry, non-sinusoidal and oscillations of current and voltage values in the arc furnace power supply system.

Keywords—electric arc furnace, hybrid Cassie–Mayr model, Chua's circuit, chaotic oscillations, subharmonic oscillations

I. INTRODUCTION

The AC electric arc furnace is a highly non-linear receiver of electrical energy, which, especially in the initial stages of steel smelting, exhibits features of chaotic dynamics. In practice, this is a very unfavorable phenomenon, manifesting itself in the continuity of the frequency characteristics of currents drawn from the supply network. Subharmonic vibrations generated in such a system lead to the development of mechanical resonances, which can be extremely dangerous to components such as transformers, synchronous machines, or even the graphite electrodes of the furnace itself due to the enormous forces acting in the system under consideration. Furthermore, chaotic current waveforms in the furnace system, via the supply line, negatively impact the power system and, consequently, the operation of parallel-connected electricity consumers.

II. ELECTRIC ARC MODEL

In the theory of electrical circuits, the arc is treated as a nonlinear resistive element. The most popular models of the dynamic voltage-current characteristics of the arc are the Cassie and Mayr models. The Cassie model of a symmetrical arc in conductance form is used to simulate processes in electrical circuits with high arc currents:

$$\frac{1}{g} \frac{dg}{dt} = \frac{1}{\theta_C} \left(\frac{u^2}{U_C^2} - 1 \right), \quad (1)$$

where: $\theta_C = h/p_{dys}$ - Cassie time constant, h - enthalpy density, p_{dys} - dissipated power density, $U_C^2 = l^2 p_{dys} / \sigma$ - Cassie voltage, l - arc length, σ - arc length. In turn, the Mayr model represents the cases of arc currents around the zero crossing much better:

$$\frac{1}{g} \frac{dg}{dt} = \frac{1}{\theta_M} \left(\frac{i^2}{g P_M} - 1 \right), \quad (2)$$

where: $\theta_M = H_0/P_M$ - Mayr time constant. A hybrid Cassie–Mayr model can be obtained in the following form:

$$g = G_{min} \left[1 - \exp\left(-\frac{i^2}{I_0^2}\right) \right] \frac{ui}{U_C^2} + \exp\left(-\frac{i^2}{I_0^2}\right) \frac{i^2}{P_M} - \theta \frac{dg}{dt} \quad (3)$$

where: G_{min} - constant conductance depending on the distance between the electrodes, I_0 - transition current between models (1) and (2), and it is assumed that the damping function $\theta = \theta_0 + \theta_1 \exp(-\alpha|i|)$.

III. MATHEMATICAL MODEL OF AN ELECTRIC ARC FURNACE

The AC steelmaking arc furnace, as a highly nonlinear consumer of electrical energy, negatively impact the power system. The development of appropriate countermeasures to limit this impact on the power supply system involves the development of an appropriate model that would sufficiently describe the chaotic nature of vibrations generated in the electric arc furnace power supply system. Using Kirchhoff's voltage and current laws, we can write equations describing the dynamics of the system under consideration:

$$\begin{cases} \frac{e_A}{n} - \frac{e_B}{n} = \left(\frac{R_{SA}}{n^2} + R_{2A} \right) i_A + \left(\frac{L_{SA}}{n^2} + L_{2A} \right) \frac{di_A}{dt} \\ \quad + M_{AB} \frac{di_B}{dt} + M_{CA} \frac{di_C}{dt} + \frac{i_A}{g_A} - \frac{i_B}{g_B} - M_{AB} \frac{di_A}{dt} \\ \quad - M_{BC} \frac{di_C}{dt} - \left(\frac{L_{SB}}{n^2} + L_{2B} \right) \frac{di_B}{dt} - \left(\frac{R_{SB}}{n^2} + R_{2B} \right) i_B \\ \frac{e_B}{n} - \frac{e_C}{n} = \left(\frac{R_{SB}}{n^2} + R_{2B} \right) i_B + \left(\frac{L_{SB}}{n^2} + L_{2B} \right) \frac{di_B}{dt} \\ \quad + M_{AB} \frac{di_A}{dt} + M_{BC} \frac{di_C}{dt} + \frac{i_B}{g_B} - \frac{i_C}{g_C} - M_{CA} \frac{di_A}{dt} \\ \quad - M_{BC} \frac{di_B}{dt} - \left(\frac{L_{SC}}{n^2} + L_{2C} \right) \frac{di_C}{dt} - \left(\frac{R_{SC}}{n^2} + R_{2C} \right) i_C \\ i_A + i_B + i_C = 0 \end{cases} \quad (4)$$

To model a very complex phenomenon, which is the unpredictable change in the length of arcs under the influence of plasma behavior in a chaotic electromagnetic field, we used Chua's system, which, despite its simplicity, generates complex chaotic oscillations:

$$\begin{cases} \frac{dx_1}{dt} = \frac{1}{a_{11}} [x_2 - x_1 - f(x_1)] \\ \frac{dx_2}{dt} = \frac{1}{a_{21}} [x_1 - x_2 + x_3] \\ \frac{dx_3}{dt} = -\frac{1}{a_{31}} [x_2 + a_{32}x_3] \end{cases}, \quad (7)$$

where: $f(x_1) = a_{13}x_1 + a_{14}(|x_1 + a_{15}| - |x_1 - a_{15}|)$.

Unpredictable changes in arc lengths must be taken into account in equation (5), where the Cassie voltage is $U_C^2 = l^2 p_{dys} / \sigma$, where the arc length in a particular phase is $l = l_0 + kx_2$.

Multi-agent Peer Review Committee for Automated Policy Analysis and Ethical Rules Enforcement*

Estera Kot

Faculty of Electrical Engineering
Warsaw University of Technology
Warszawa, Poland
estera.kot@pw.edu.pl

Santhosh Kumar Ravindran

Microsoft
Azure Data
Redmond, WA, USA
Santhosh.Ravindran@microsoft.com

Weronika Nitecka

School of Public Affairs
Sciences Po
Paris, France
weronika.nitecka@sciencespo.fr

Krzysztof Siwek

Faculty of Electrical Engineering
Warsaw University of Technology
Warszawa, Poland
krzysztof.siwek@pw.edu.pl

Zuzanna Krawczyk-Borysiak

Faculty of Electrical Engineering
Warsaw University of Technology
Warszawa, Poland
zuzanna.krawczyk@pw.edu.pl

Abstract—Privacy policy compliance presents a fundamental computational challenge in distributed enterprise systems: while regulatory frameworks mandate comprehensive policy disclosure, empirical evidence demonstrates systematic user non-engagement with policy documents, creating information asymmetries that enable exploitative data practices. Our systematic analysis of 100 high-traffic platforms across social media, e-commerce, and gaming domains reveals pervasive explicit third-party data monetization clauses, highlighting the inadequacy of current reactive compliance mechanisms. We propose a distributed multi-agent system architecture implementing automated policy analysis through coordinated peer review protocols. The system instantiates five specialized agents utilizing large language models with domain-specific fine-tuning: (1) a Policy Security Agent implementing threat modeling and vulnerability assessment algorithms, (2) a Policy Review Agent performing semantic analysis and compliance mapping, (3) a Policy Validation Supervisor Agent with cross-domain knowledge graphs for holistic policy evaluation, (4) a Hallucination Control Agent implementing consistency verification through adversarial validation, and (5) a Metadata Logging Agent maintaining comprehensive provenance chains for audit trail generation. The architecture implements a consensus-based validation protocol where agents perform iterative cross-validation to minimize false positives and ensure policy interpretation accuracy. Our approach addresses the temporal gap between policy violation detection and enforcement through real-time monitoring agents that continuously analyze system logs, user behavior patterns, and data flow trajectories across distributed enterprise infrastructure. Key technical contributions include: (1) a novel multi-agent consensus protocol for policy interpretation with formal verification properties, (2) real-time anomaly detection algorithms for policy violation identification, (3) explainable AI mechanisms providing complete decision provenance for regulatory audit requirements, and (4) adaptive learning protocols enabling continuous model improvement through human feedback integration.

The distributed architecture scales horizontally with enterprise infrastructure growth while maintaining sub-linear computational complexity. Human-in-the-loop integration protocols preserve organizational authority over policy enforcement while leveraging machine intelligence for continuous improvement through reinforcement learning mechanisms. This work addresses critical gaps in automated governance systems by provid-

ing formal verification properties, explainable decision-making, and real-time enforcement capabilities. The multi-agent approach represents a paradigm shift from reactive compliance auditing to proactive policy enforcement through intelligent automation.

Index Terms—Multi-agent systems, Natural language processing, Policy compliance automation, Explainable artificial intelligence, Distributed systems, Real-time anomaly detection

Multi-Task Learning and its Optimization

A Study of Instance-Wise Risk Minimization and Joint Object Detection with Classification

Karol Wojciechowski*

Warsaw University of Life Sciences,
Warsaw, Poland

karol.wojciechowski.it@gmail.com

Bartosz Świdorski

Department of Artificial Intelligence,
Institute of Information Technology,
Warsaw University of Life Sciences

Warsaw, Poland

bartosz_swidorski@sggw.edu.pl

Maciej Jurewicz

Department of Artificial Intelligence,
Institute of Information Technology,
Warsaw University of Life Sciences

Warsaw, Poland

maciej_jurewicz@sggw.edu.pl

Grzegorz Gwardys

Faculty of Electronics and Information Technology,
Warsaw University of Technology,
Warsaw, Poland

grzegorz.gwardys@gmail.com

Abstract—Multi-task learning (MTL) aims to jointly optimize multiple objectives within a single model by exploiting shared representations. In this work we investigate two related but distinct multi-objective setups in the context of two-stage object detectors: (1) *Instance-Wise Risk Minimization* (IWRM), where each training example defines a separate objective, and (2) a classical MTL scenario where a detector performs both localization (detection) and an auxiliary per-instance classification task. Building on Detectron2’s Faster R-CNN with a Feature Pyramid Network (FPN) backbone, we augment the standard ROI processing pipeline with a lightweight auxiliary classification head attached to the shared box-head features. This design preserves maximal parameter sharing: pooled ROI features are processed by the box head into a per-ROI vector h , and three parallel linear predictors map h to (i) detection logits, (ii) bounding-box deltas, and (iii) auxiliary class logits. Training optimizes the usual RPN + detection losses together with an auxiliary cross-entropy term for positive proposals.

A central methodological focus is gradient aggregation. We compare the baseline strategy of simple averaging (or static weighting) of task losses with Jacobian Descent (JD) using the AUPGrad aggregator introduced by Quinton & Rey. JD treats the per-task gradients as rows of a Jacobian matrix J and computes a conflict-resolving update by projecting and averaging in the task space; computationally efficient variants operate on the small Gram matrix $G = JJ^T$ and offer stochastic subsampling for large objective counts. We implement both aggregation pipelines inside Detectron2 (collecting flattened per-task gradients, forming J , computing the aggregated update and scattering it back to parameters) and instrument training with diagnostic metrics: per-task losses, cosine similarities between task gradients (pre/post aggregation), and aggregated update alignments.

Empirical evaluation uses two custom datasets: an agricultural drone dataset for IWRM-style instance segmentation (converted to Detectron2 format) and a medical imaging dataset for joint detection + per-ROI classification (three classes). Key findings are: (1) AUPGrad accelerates early convergence in the IWRM setting while producing final bounding-box and mask AP comparable to the averaged baseline, with modest overhead due to small-dimensional Gram solves; (2) in the classical MTL case, most detection–classification gradient pairs were non-conflicting and averaging performed as well or better — AUPGrad introduced 30% training overhead and did not improve, and sometimes reduced, inference performance; (3) diagnostics (loss curves and cosine similarities) are crucial to decide whether a principled aggregator is warranted for a given tasks.

We conclude that Jacobian Descent (AUPGrad) is a valuable tool for IWRM and other conflict-heavy multi-objective scenarios, but its benefits in standard MTL (detection + auxiliary

classification) are task dependent. We recommend practitioners instrument gradient alignment metrics and to consider stochastic/blocked JD variants when scaling to many objectives. Source code modifications, experimental logs and visual diagnostics are discussed in the full paper.

Index Terms—Multi-task learning, Jacobian Descent, Gradient Descent, AUPGrad, Detectron2, Faster R-CNN, Instance-Wise Risk Minimization

On generation of adversarial sequences for recurrent neural networks in classification and forecasting

Rafał Zan

Warsaw University of Technology

Warsaw, Poland

rafal.zan.stud@pw.edu.pl

Bartosz Chaber

Warsaw University of Technology

Warsaw, Poland

bartosz.chaber@pw.edu.pl

Abstract—One of the emerging problems associated with neural networks is their resilience to adversarial input data.

This paper focuses on recurrent neural networks (RNN), like Long Short-Time Memory networks (LSTM) or Nonlinear AutoRegressive networks with eXogenous inputs (NARX). It shows how one might prepare some malicious input data to make the trained neural network produce wrong answers. This paper aims to analyze such manipulations' impact on RNN-based networks. The article will include a comprehensive study of which gradient-based and non-gradient-based data manipulation techniques are possible.

An LSTM network will be used for a classification task of a text sequence, but a similar approach might be applied to electrical signals or network traffic data. Due to the discrete nature of the sequence tokens, it covers techniques based on synonymization, token removal, or random token insertion. A technique leveraging the BERT model to search for more context-aware synonyms is presented.

This paper adapts methods like Projected Gradient Descent (PGD) to generate adversarial sequences of tokens. The mentioned method allows using a gradient of the model's loss function to discover optimal token perturbations. This article shows the results of experiments on how different word embeddings (like GloVe or Word2Vec) affect the model's performance and accuracy.

Final findings suggest that LSTM models exhibit greater resistance to subtle input changes (using synonyms) than standard RNNs but remain susceptible to more advanced attacks. The research shows that crafting an adversarial sequence of tokens is inherently more complex than crafting a malicious image data or a time series. However, it is still feasible and can result in successful model misclassification.

The second part of the paper focuses on recurrent neural networks for a forecasting task. A NARX model is trained to predict the sensor readings of a simple ventilation system. The input to the model is a control signal with an electric valve states. This model is a troublesome due to its recurrent connections. An Automatic Differentiation is used for efficient calculation of the gradient with respect to the input control signal. The Forward Accumulation Automatic Differentiation presents itself as a viable option for a fast calculation of such a gradient. This derivatives might be useful at determining how the input signal have to be modified in order to change the predicted values significantly.

Index Terms—recurrent neural network, adversarial attack, NARX, LSTM

I. INTRODUCTION

Recurrent Neural Networks (RNN) and their other variants such as Long-Short Term Memory or Gated Recurrent Units have become one of the fundamental tools in Natural Language Processing due to their ability to accurately model sequential dependencies both in textual and visual data. These models are especially well-suited for image processing and sentiment analysis where the goal is to determine the emotions expressed behind user-generated content on social media posts, reviews or feedback. Despite their effectiveness, RNN-based models might still be vulnerable to deliberate perturbations introduced to the input data that can significantly affect how the network might classify the input, or predict the next output value in the sequence.

A. Text-based Recurrent Neural Network classifier

Difficulty of crafting an adversarial input for text-based recurrent neural networks stems from the fact that text data is inherently discrete, in the sense that each token (i.e. word) in the sequence (i.e. sentence) often comes from a finite vocabulary. This is what complicates the generation process of adversarial examples without disrupting the grammatical structure or semantic coherence.

B. Recurrent neural network for forecasting

Many behavioral models in electrical engineering benefit from an RNN-based model. Given a few past input signal values, and a few past output signal values, a trained recurrent neural network can predict the next output signal value. The input signal often consists of some control parameters, while the output signal contains a set of sensor readings. The recurrent nature of RNNs makes it more difficult to craft an adversarial signal, as calculating a derivative of the loss functions of such a network requires a special care and proper choice of automatic differentiation algorithms to unroll the recurrence.

II. RESULTS

By using an iterative algorithm of Progressive Gradient Descent (PGD), we were able to select the most influential word in the sentence and switch it to change the classifier output. For a forecasting RNN, we have used a Forward-mode Automatic Differentiation to find the time instant at which the model is the most sensitive to the input signal.

Secondary Electron Emission modeling for 2nd Townsend Coefficient estimation in Julia/CUDA

1st Wiktor Łodyga
Faculty of Electrical Engineering
Warsaw University of Technology
Warsaw, Poland
wiktor.lodyga@pw.edu.pl

2nd Bartosz Chaber
Faculty of Electrical Engineering
Warsaw University of Technology
Warsaw, Poland
bartosz.chaber@pw.edu.pl

3rd Jacek Starzyński
Faculty of Electrical Engineering
Warsaw University of Technology
Warsaw, Poland
jacek.starzynski@pw.edu.pl

Abstract—In this work, we present a numerical approach to estimate the effective second Townsend coefficient for argon discharges interacting with copper electrodes. The approach uses a Particle-in-Cell (PIC) model combined with Monte Carlo collisions (MCC) for gas-particle interactions. To enable the evaluation of γ , a custom boundary condition is introduced, with an additional Monte Carlo process to model the emission of secondary electrons in the domain, triggered by ion impacts on the electrode surface. The model is implemented in Julia programming language and parallelized using CUDA for efficient execution on GPUs.

Index Terms—Secondary Electron Emission, Townsend coefficient, Monte Carlo Collisions, Particle-in-Cell, Julia programming language, GPU programming

I. INTRODUCTION

When an electric field is applied across a gas gap, free electrons drift towards the anode, colliding with neutral atoms and molecules. If the field is sufficiently strong, electrons gain enough energy between collisions to ionize neutrals, producing an avalanche of secondary electrons.

Ionization alone cannot sustain a discharge: electrons lost to the anode must be replenished near the cathode. At higher fields, incident ions release electrons from the cathode surface via secondary electron emission (SEE). Together, avalanche ionization and SEE enable a self-sustaining discharge, known as a Townsend discharge, provided the criterion

$$\gamma(e^{\alpha d} - 1) = 1 \quad (1)$$

is satisfied, where α is the first Townsend coefficient and γ the effective SEE coefficient.

The breakdown voltage V_b in the Townsend regime is often described by Paschen's law,

$$V_b = \frac{Bpd}{\ln(Apd) - \ln\left(\ln\left(1 + \frac{1}{\gamma}\right)\right)}, \quad (2)$$

which relates V_b to the product of pressure p and gap distance d . The empirical coefficients A and B depend on the gas, while γ accounts for secondary electron emission. Despite its usefulness, this relation neglects detailed electron kinetics and surface effects, and is therefore unreliable outside well-studied conditions.

Particle-in-cell/Monte Carlo collision (PIC/MCC) simulations overcome these limitations by directly resolving electron kinetics and collisional processes, allowing first-principles calculation of α and effective γ [2]–[5].

In this work, we simulate a low-pressure argon discharge between copper electrodes. Electrons and ions are modeled as superparticles moving in self-consistent fields, undergoing elastic, excitation, and ionization collisions with cross sections from LXCat [8]. The SEE yield at the cathode is described by an energy-dependent function [5]–[7],

$$\gamma(E) = \gamma_{\max} \cdot \frac{E/E_{\max}}{1 + (E/E_{\max})^2}, \quad (3)$$

where E is the ion impact energy, and γ_{\max} , E_{\max} are material-dependent parameters.

The code is implemented in Julia [9] with CUDA acceleration for field solving, particle pushing, and collisions.

REFERENCES

- [1] J. Townsend, *Electricity in Gases*. Oxford: Clarendon Press, 1915.
- [2] A. Derzsi, I. Korolov, E. Schüngel, Z. Donkó, and J. Schulze, "Effects of fast atoms and energy-dependent secondary electron emission yields in PIC/MCC simulations of capacitively coupled plasmas," *Plasma Sources Sci. Technol.*, vol. 24, no. 3, p. 034002, 2015.
- [3] A. Derzsi, R. Masheyeva, F. Beckfeld, J. Schulze, and Z. Donkó, "Determination of the effective secondary electron emission coefficient for low-pressure RF discharges," 2024.
- [4] M. S. Mokrov and Yu. P. Raizer, "Monte Carlo method for finding the ionization and secondary emission coefficients and I–V characteristic of a Townsend discharge in hydrogen," *Tech. Phys.*, vol. 53, no. 4, pp. 436–444, 2008.
- [5] Z. J. Ding, X. D. Tang, and R. Shimizu, "Monte Carlo study of secondary electron emission," *J. Appl. Phys.*, vol. 89, no. 1, pp. 718–726, 2001.
- [6] A. Shih, J. Yater, C. Hor, and R. Abrams, "Secondary electron emission studies," *Appl. Surf. Sci.*, vol. 111, pp. 251–258, 1997.
- [7] M. Furman and M. Pivi, "Probabilistic model for the simulation of secondary electron emission," *Phys. Rev. ST Accel. Beams*, vol. 5, no. 12, p. 124404, 2002.
- [8] S. Pancheshnyi, S. Biagi, M. Bordage, G. Hagelaar, W. Morgan, A. Phelps, and L. Pitchford, "The LXCat project: Electron scattering cross sections and swarm parameters for low temperature plasma modeling," *Chem. Phys.*, vol. 398, pp. 148–153, 2012.
- [9] J. Bezanson, A. Edelman, S. Karpinski, and V. B. Shah, "Julia: A Fresh Approach to Numerical Computing," *SIAM Rev.*, vol. 59, no. 1, pp. 65–98, 2017.

Simplified Information Coding System for Use in Emergencies

Dmitro Trushakov
*Department of Automation
of Production Processes*
Central Ukrainian National Technical
University
Kropyvnytskyi, Ukraine
0000-0003-0326-2383

Serhiy Rendzinyak
*Faculty of Electronics and
Computer Technologies*
Ivan Franko National
University of Lviv
Lviv, Ukraine
0000-0003-4544-4871

Oleksandr Kozlovskiy
*Department of Electrical Systems and
Energy Management*
Central Ukrainian National Technical
University
Kropyvnytskyi, Ukraine
0000-0001-6885-5994

Ruslan Teliuta
*Department of Electrical Systems and
Energy Management*
Central Ukrainian National Technical
University
Kropyvnytskyi, Ukraine
0000-0002-4923-1227

Vasyl Korud
*Institute of Power Engineering and
Control Systems*
Lviv Polytechnic National University
Lviv, Ukraine
0000-0002-1289-3534

Marianna Fedotova
*Department of Automation
of Production Processes*
Central Ukrainian National Technical
University
Kropyvnytskyi, Ukraine
0000-0002-5827-1685

Abstract—The primary objective of this work is to develop a straightforward and user-friendly method for encoding information for subsequent transmission as digital information messages. In this case, it is necessary to provide the smallest number of code combinations that will allow the fastest transmission of information messages and the timely receipt of the information required by the recipient in emergencies, for example.

Such information must be transmitted in encoded form. Currently, there are many different encoding methods. The most famous optimal codes are the Shannon-Fano coding and the Huffman coding algorithm.

The proposed method is based on the principle of transliteration of the Ukrainian alphabet (32 letters) into the Latin alphabet (26 letters). In addition to the letters, at least three more symbols are also required – a space between words, a comma, and a full stop. As a result of performing actions according to this algorithm, the resulting code becomes uneven but optimal.

In this regard, there are disadvantages, namely, in non-uniform codes, when decoding information messages to the original state, there are difficulties in detecting the message boundary. Therefore, to eliminate errors, it is also necessary to use special separators. That is, when using the Shannon-Fano coding to transmit information messages, the use of special separators reduces the speed of information transmission and complicates the decryption process. In addition, the Shannon-Fano coding technique may not always lead to the correct construction of the code, since when dividing into subgroups, both the upper and lower subgroups can be made more likely.

The Huffman coding technique allows you to obtain the correct construction of the code with a smaller average number of symbols per letter for a given probability distribution.

The information message is encoded as follows: first, the process of transliteration from Cyrillic to Latin occurs; then, the process of assigning each letter of the Latin alphabet the corresponding code combination begins. After the encoding process is completed, the information message is transmitted to the communication line to the digital information receiver. Sometimes extraneous noise (the so-called interference) occurs on the communication line, so the information message is

cleared of interference in the digital filter. Then the information message is decoded in the decoder and is sent to the user in its usual form. As the simplest device for displaying the received information message, the nRF24L01 radio module and the 1602 LCD from the ARDUINO microprocessor set were used.

The coding method, algorithm, and structural diagram of the information encoding and transmission process have been developed. The created information encoding system allows you to speed up the process of transmitting information in encoded form, which is especially relevant during emergencies.

Study of Digital Twin Technology for SCADA System Simulation and Analysis

Nomin Lkhgvasuren
SCADA Engineer of MCS International
Mongolian University of Science and Technology
Ulaanbaatar, Mongolia
nomin.l@mcsi.mn

Wolfram Hardt
Department of Computer Engineering
Technische Universität Chemnitz
Chemnitz, Germany
wolfram.hardt@informatik.tu-chemnitz.de

Zagdkhorol Bayasgalan
Power Engineering School
Mongolian University of Science and Technology
Ulaanbaatar, Mongolia
zagdkhorol@must.edu.mn

Uranchimeg Tudevdaeva
Graduate School
Mongolian University of Science and Technology
Ulaanbaatar, Mongolia
uranchimeg@must.edu.mn

Abstract—This paper presents a study on applying Digital Twin technology to simulate pump operations within a SCADA-controlled water supply system. Without direct real-time data access, the approach relies on manually extracting historical data from the SCADA historian to recreate pump behavior in a virtual environment. Key operational variables—such as flow rate, pressure, and motor status—are modeled to analyze performance patterns and detect possible anomalies. Although the Digital Twin model is operated offline, this method offers valuable insights into system behavior and demonstrates the potential of Digital Twins for enhancing predictive maintenance and operational decision-making. The study lays a foundation for future integration efforts aimed at achieving real-time synchronization and more dynamic system monitoring.

Keywords—*pump operation, historical data, offline simulation, predictive maintenance, performance analysis, virtual modeling*

Classification of SSVEP Using a Subject-Independent Approach for Brain-Computer Interface Applications

Przemysław Wiszniewski
Warsaw University of Technology
Faculty of Electrical Engineering
ul. Koszykowa 75, 00-662 Warsaw, Poland
ORCID: 0000-0002-2336-841X
przemyslaw.wiszniewski.dokt@pw.edu.pl

Marcin Kołodziej
Warsaw University of Technology
Faculty of Electrical Engineering
ul. Koszykowa 75, 00-662 Warsaw, Poland
ORCID: 0000-0003-2856-7298
marcin.kolodziej@pw.edu.pl

Andrzej Majkowski
Warsaw University of Technology
Faculty of Electrical Engineering
ul. Koszykowa 75, 00-662 Warsaw, Poland
ORCID: 0000-0002-6557-836X
andrzej.majkowski@pw.edu.pl

Abstract— This study investigates the feasibility of reliably classifying steady-state visually evoked potential (SSVEP) signals in a subject-independent setting using a support vector machine (SVM) classifier. Specifically, it evaluates the effectiveness of training the classifier exclusively on data from users other than the one whose data are used for testing. This approach aims to reduce or even eliminate the need for user-specific calibration, thereby increasing the practicality and scalability of brain-computer interface (BCI) applications in real-world settings.

Keywords: SSVEP, SVM, subject-independent classification

I. INTRODUCTION

Steady-state visual evoked potentials (SSVEPs) are among the fundamental methods used in brain-computer interface (BCI) systems [1], [2]. They are elicited in electroencephalography (EEG) signals when a subject is exposed to a light source flashing at a constant frequency [3]. A major challenge in SSVEP-based BCIs is the variability of EEG signals, both across different subjects and between sessions of the same subject [4], [5], [6]. This variability complicates the design of reliable and generalizable BCI systems. Traditional approaches often rely on user-specific calibration, which is time-consuming and reduces the practical usability of BCIs. Consequently, there is growing interest in subject-independent classification methods that can perform effectively without requiring individualized adjustments.

II. MATERIALS AND METHODS

The purpose of EEG recording in this study was to elicit steady-state visually evoked potentials (SSVEPs) through the use of visual stimuli at specific frequencies. A total of 15 recordings were conducted, one for each of the 15 participants. Each recording lasted 60 seconds and involved exposure to visual stimuli at frequencies of 7, 8, and 9 Hz. The stimuli were generated by an LED matrix measuring 65×65 mm, positioned 1 m from the participants' eyes. The brightness of the LEDs was adjusted to ensure comfort and to avoid visual fatigue. EEG signals were recorded using a g.USBamp 2.0 amplifier (g.tec) with 24-bit A/D converters and a sampling rate of 256 Hz. Electrodes were placed on the scalp according to the international 10–20 system. To simplify data analysis and to provide an initial assessment of the proposed approach, only the signal from electrode Oz was used.

EEG signals were preprocessed using a 4th-order Butterworth band-pass filter with a passband of 0.1–45 Hz. The purpose of filtering was to suppress low-frequency baseline drifts and high-frequency artifacts, including power-line interference. Furthermore, the data was normalized. This approach enabled the evaluation of classifier performance under conditions of minimal interference with the input signal.

Feature extraction was then performed using spectral analysis with the Fourier transform. Each segment of 256 samples (1 second) was transformed via the FFT algorithm into 256 complex values. The magnitudes (amplitudes) were computed, yielding a frequency-domain representation of the signal with a resolution of 1 Hz.

III. RESULTS AND DISCUSSION

In the first approach to training the SVM classifier, a leave-one-subject-out (LOSO) strategy was applied. In each iteration, the training process was performed on data from 14 participants, while testing was carried out on data from the remaining participant. The procedure was repeated multiple times, each time designating a different participant as the test subject, so that each of the 15 participants served as the test set exactly once. The analysis of results shows that the SVM method achieved the highest average accuracy among all compared approaches, reaching 78.49%. In many cases, classification accuracy exceeded 90%.

IV. CONCLUSIONS

The conducted experiments confirm that subject-independent classification of SSVEP signals can achieve high accuracy, making it possible in practice to eliminate the need for session-specific calibration. These findings have significant implications for the practical deployment of BCI systems. Future research should focus on enhancing the generalizability and robustness of such models across diverse users and environments.

REFERENCES

- [1] S. Saha *et al.*, “Progress in Brain Computer Interface: Challenges and Opportunities,” *Front Syst Neurosci*, vol. 15, p. 578875, 2021, doi: 10.3389/fnsys.2021.578875.
- [2] J. R. Wolpaw, N. Birbaumer, D. J. McFarland, G. Pfurtscheller, and T. M. Vaughan, “Brain-computer interfaces for communication and control,” *Clinical Neurophysiology*, vol. 113, no. 6, pp. 767–791, Jun. 2002, doi: 10.1016/S1388-2457(02)00057-3.
- [3] M. Łabęcki, M. M. Nowicka, A. Wróbel, and P. Suffczynski, “Frequency-dependent dynamics of steady-state visual evoked potentials under sustained flicker stimulation,” *Sci Rep*, vol. 14, no. 1, p. 9281, Apr. 2024, doi: 10.1038/s41598-024-59770-5.
- [4] R. C. Maswanganyi, C. Tu, P. A. Owolawi, and S. Du, “Statistical Evaluation of Factors Influencing Inter-Session and Inter-Subject Variability in EEG-Based Brain Computer Interface,” *IEEE Access*, vol. 10, pp. 96821–96839, 2022, doi: 10.1109/ACCESS.2022.3205734.
- [5] H.-Y. Zhang, C. E. Stevenson, T.-P. Jung, and L.-W. Ko, “Stress-Induced Effects in Resting EEG Spectra Predict the Performance of SSVEP-Based BCI,” *IEEE Transactions on Neural Systems and Rehabilitation Engineering*, vol. 28, no. 8, pp. 1771–1780, 2020, doi: 10.1109/TNSRE.2020.3005771.
- [6] A. Melnik *et al.*, “Systems, Subjects, Sessions: To What Extent Do These Factors Influence EEG Data?,” *Front Hum Neurosci*, vol. 11, p. 150, Mar. 2017, doi: 10.3389/fnhum.2017.00150.

Survey on Racing simulators as an environment for reinforcement learning

1st Jacek Wójtowicz

¹*Faculty of Electrical Engineering
Warsaw University of Technology*

²*SBL - Instytut Elektrotechniki
Warsaw, Poland*

jacek.wojtowicz2.dokt@pw.edu.pl
ORCID 0009-0007-0109-0916

2nd Krzysztof Siwek

*Faculty of Electrical Engineering
Warsaw University of Technology
Warsaw, Poland*

krzysztof.siwek@pw.edu.pl
ORCID 0000-0003-2642-2319

In recent years, there has been a rapid development of artificial intelligence and machine learning methods, which has resulted in the creation of increasingly advanced autonomous vehicles. Along with the development of this field of the automotive industry, Motorsport related to this field slowly begins its development.

In 2021, the first Indy Autonomous Challenge took place, during which autonomous cars took part in challenges such as: completing a full lap on time, passing an obstacle at the highest possible speed and overtaking another vehicle. In 2024, the first Abu Dhabi Autonomous Racing League competition was held. The competition consisted of challenges similar to the Indy Autonomous Challenge. In addition, a full-fledged race (of all cars at the same time) consisting of 8 laps was also held.

The structure of the autonomous vehicle control system can be divided into 3 main stages: Perception, Planning and Control. Perception and Planning have been explored for a long time, but the Control stage is only developing now, when Perception and Planning are at a sufficient level for the vehicle to move independently to some extent. Autonomous vehicle racing is great for developing this area because during the race, the car is expected to use its full potential at almost every turn. This requires an advanced control system that will be able to properly match the vehicle's speed to the trajectory of movement while also taking into account variable conditions such as tire wear, brake wear, or changing weather conditions.

Previous stages as Perception and Planning are currently strongly based on a Convolutional Neural Network (CNN). Machine learning in these areas has been possible thanks to a massive amount of photos and recordings from regular human-driven vehicles. The data necessary for CNN training are easily accessible and widely distributed.

Unfortunately it cannot be said about data essential to train neural network to control the car in a safely manner. As previously mentioned, the only place where such data could be collected is a race track, where vehicles reach their limits. Collecting data that way is highly expensive, since the car, experience driver and data measurement system is needed.

Racing simulators are very good alternative for both collect-

ing necessary training data and environment for reinforcement learning approach. It is also worth to mention, that in both competitions, Indy Autonomous Challenge and Abu Dhabi Autonomous Racing League competitors must complete qualification in simulations.

Reinforcement learning (RL), particularly deep reinforcement learning (DRL), is especially promising in the context of autonomous vehicle control, where decision-making needs to be continuously adjusted based on the environment and vehicle state. In contrast to supervised learning, where predefined datasets are used, RL enables an agent to learn optimal control policies through interaction with a simulated environment by maximizing cumulative rewards. This makes it particularly well-suited for scenarios like autonomous racing, where control decisions must account for high-speed dynamics, collision avoidance, and real-time adaptation to track and opponent behaviour. Furthermore, RL is capable of discovering novel driving strategies that are not present in human data, which is valuable in pushing performance limits. Techniques such as Proximal Policy Optimization (PPO), Deep Q-Networks (DQN), and Soft Actor-Critic (SAC) have already been successfully applied in various autonomous driving simulation environments. The use of curriculum learning, domain randomization, and sim-to-real transfer further enhances the potential of RL-based systems to be generalizable and robust when deployed on real race tracks.

In this article commercial racing simulators and simulators specially designed for neural network learning purpose will be presented.

First, they will be analyzed and evaluated for their ability to replicate real-world vehicle behavior and the effects of weather, road surface, and vehicle component wear if implemented on driving characteristics.

Second, possible add-ons and already implemented functions for AI or machine learning will be described and assessed for their usefulness and width of applications.

Finally, existing applications of using racing simulators to train neural networks will be presented.

Three-State Monitoring Circuit for Sensor Operation in Automation Systems

Agnieszka Choroszucho

Department of Electrotechnics, Power
Electronics and Electrical Power
Engineering, Faculty of Electrical
Engineering
Białystok University of Technology
Białystok, Poland
a.choroszucho@pb.edu.pl

Norbert Waśkiewicz

Faculty of Electrical Engineering
Białystok University of Technology
Białystok, Poland
norbert.waskiewicz.109529@student.p
b.edu.pl

Jacek Maciej Stankiewicz

Faculty of Electrical Engineering
Białystok University of Technology
Białystok, Poland
jacek.stankiewicz@sd.pb.edu.pl

Abstract— In demanding industrial environments, detection sensors are exposed to various risk factors such as mechanical stress, environmental fluctuations (temperature, humidity, dust), and electrical disturbances including voltage spikes or overloads. These conditions often lead to partial or total sensor failure, which may not be immediately visible through conventional diagnostic approaches. Traditional monitoring systems typically rely on reading the binary output state of a sensor, which does not allow for distinguishing between normal operation, sensor activation, or a complete disconnection or malfunction.

To address these limitations, a compact and cost-effective monitoring circuit has been developed that extends diagnostic capabilities by analyzing the sensor's current consumption. This approach introduces a three-state diagnostic model: (1) idle but functional sensor, (2) active detection state, and (3) fault condition due to damage or disconnection. Each state is identified by characteristic current profiles, which are easily distinguishable by the circuit, enabling clear fault detection at

the hardware level without the need for digital processing or advanced software diagnostics.

The circuit is implemented using basic analog components and visual indicators, such as LEDs, making it suitable for integration into existing systems without significant design modifications or computational overhead. Moreover, its low complexity and real-time response make it especially useful in environments where maintenance access is limited or where downtime must be minimized.

The proposed solution enhances the reliability and maintainability of sensor-based systems in automation and power electronics applications. It can be particularly valuable in safety-critical systems, where early detection of sensor failure is essential to maintaining operational continuity and preventing damage or hazards

Wavelet Transform denoising in application for EM field signal acquisition

Adam JÓSKO

Faculty of Electrical Engineering
Warsaw University of Technology
Warsaw, Poland

adam.josko@pw.edu.pl; ORCID:0000-0003-4093-6252

Jacek STARZYŃSKI

Faculty of Electrical Engineering
Warsaw University of Technology
Warsaw, Poland

jacek.starzynski@pw.edu.pl; ORCID: 0000-0002-1093-9500

Abstract—The paper contains continuation of the Authors' research in the field of the procedure development for the signals acquired by the derivative EM field probes. The problem is presented based on the E field measurement but it is exactly the same as the M field is measured.

Index Terms—derivative probes, signal processing, signal integration, wavelet transform, wavelet denoising

I. INTRODUCTION

A. Background Idea

The recording of temporal variations of the Electric and/or Magnetic field, often produces a raw signal that requires dedicated post-processing. In the standard approach, this procedure involves the removal of the DC component followed by signal integration. The integrated signal may still exhibit strong trend-like components, which in practice hinder reliable analysis (Fig. 1). The present paper introduces and discusses original solutions proposed by the authors to overcome this challenge.

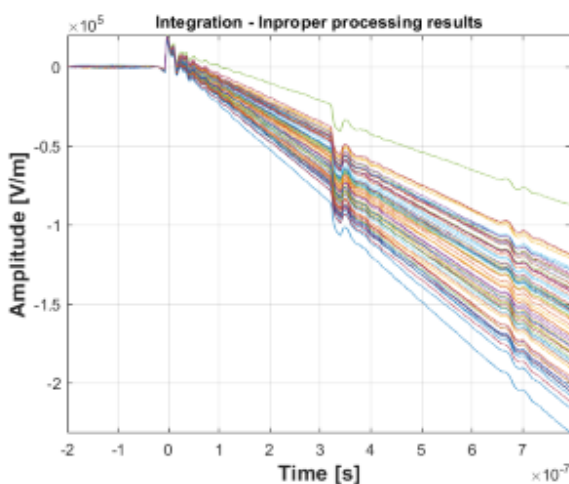


Fig. 1. Possible integration result.

The work is supported by the within the project "Development of signal conditioning methods in electric and magnetic field measurements" WUT, "Opracowanie metod kondycjonowania sygnałów w pomiarach pola elektrycznego i magnetycznego", RND AEEITK PW

B. Tools and Possibilities

The authors decided to modify the classical approach involving only the DC component, extending it to also account for slowly varying components. Their initial idea was to apply temporal segmentation of the raw signal representing the field variations [1]. However, the method did not sufficiently facilitate the automation of the processing procedure. For this reason, the authors turned to the Wavelet Transform, whose inherent time–scale characteristics allow joint analysis in both the time and frequency domains. Preliminary observations and results were reported in [2]. Wavelets allow for signal decomposition into frequency subbands also including slow varying components. They can be removed in the following stages. The resulting processed signals are presented in this work (Fig. 2).

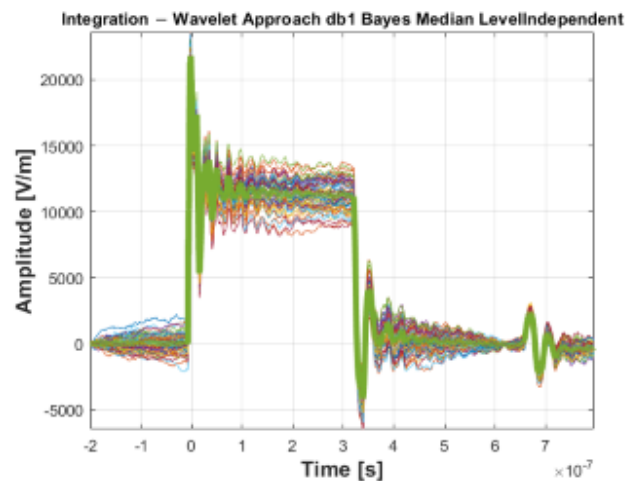


Fig. 2. Example of a wavelet based integration result.

REFERENCES

- [1] Dziadak Bogdan, Starzyński Jacek, Sroka Jan, Jósko Adam: Derivative Probes Signal Integration Techniques for High Energy Pulses Measurements, *Energies*, vol. 15, nr 6, 2022, s. 2244, DOI:10.3390/en15062244
- [2] Adam Jósko;Jacek Starzyński: Wavelets Application for Derivative Probes Signal Integration Procedures, 2024 25th International Conference on Computational Problems of Electrical Engineering (CPEE)